NTNU – Trondheim
Norwegian University of
Science and Technology

Optical dip probes for near-infrared spectroscopic glucose sensing in peritoneal fluid

Petter Rossvoll

Master of Science in Cybernetics and Robotics
Submission date: Januar 2015
Supervisor: Øyvind Stavdahl, ITK
Co-supervisor: Anders Lyngvi Fougner, ITK

Norwegian University of Science and Technology
Department of Engineering Cybernetics

Assignment text

The Department of Engineering Cybernetics at NTNU has recently established the Artificial Pancreas Trondheim (APT) research group in cooperation with St Olavs Hospital and Faculty of Medicine at NTNU. In this assignment you are to design, assess and model a glucose sensor system suitable for APT's approach for glucose control.

1. Give a brief presentation of the glucose and insulin dynamics in humans with diabetes mellitus type 1 or 2, as well as in humans without diabetes. Describe sensor types suitable for measuring glucose concentration in blood plasma. Give special attention to near-infrared (NIR) sensors.

2. Using available NIR sensors and optical transflectance dip probes, collect spectral data based on peritoneal fluid of various glucose concentrations.

3. Apply multivariate calibration techniques for analysis of the spectral data in order to:
   a) Identify particular spectral regions useful in determining sample glucose level.
   b) Assess the dip probe's performance in peritoneal fluid samples.

4. If time permits, compare the results from dip probe experiments with other NIR measurement methods (e.g. Raman spectroscopy). Discuss the results in terms of clinical relevance.

Contents

List of Figures

List of Tables

Abstract

The aim of this study was to investigate the possibilities of using near infrared spectroscopic measurements to detect and quantify glucose concentration in peritoneal fluid samples. This was done with a fibre dip probe in samples obtained from patients at St. Olavs Hospital. The measurements was done by transflection in small sample volumes, hoping to shed some light the eventual future application of this method in an implantable glucose sensor. The acquired spectra were analysed with the use of the multivariate calibration techniques PCA and PLSR. Particular useful wavelengths were identified by MW-PLSR.

1 Introduction

The ability to control blood glucose level is vital. Both hypoglycaemia and hyperglycaemia are conditions which untreated may lead to coma and death. Diabetes is classified as an epidemic, and the number of diabetics grows fast globally. The number of diabetics world wide are currently estimated to 387 million, and to reach 592 million by 2035 [1].

Today, diabetic patients rely on self monitoring of glucose levels. Often by subcutaneous measurement of glucose concentration in the interstitial fluid. This is a method with great uncertainty in the prediction of the actual blood glucose (BG) concentration. These methods also rely on calibration by finger-prick methods (2-4 times daily), which measures a small sample of blood, usually drawn from the tip of the finger. For the last decades a goal has been to develop a noninvasive method for determination of BG. As this will ease the life of diabetics significantly. The research has nearly exclusively focused on NIR measurement in the subcutaneous tissue [2]. There is a race going on in the development towards the first safe, reliable and clinically approved device for non-invasive BG measurement.

However, these methods rely on the indirect prediction of BG through readings in the interstitial fluid. The interstitial glucose levels experience a significant delay in reflecting BG levels when compared to intravenous measurement. The reported delay varies between 10 min to 45 min.

An artificial pancreas seeks to solve the diabetics lack of effective glucose regulation. Thus it must utilize a reliable mode of measurement and a safe way of administrating insulin release. This gives the rationale behind looking at the peritoneum to meet both these requirements. The peritoneum is reported to offer faster BG kinetics [3]. And it is a faster at taking up delivered insulin [4].

This work investigates the possibility for measuring BG in peritoneal fluid. We apply a near infrared spectrophotometer equipped with a fibre dip probe

to measure directly in peritoneal fluid samples. The samples are drawn from patients at St. Olavs Hospital and analysed ex-vivo.

The development of near infrared spectroscopy are closely related to the development of multivariate calibration techniques. And especially principal component analysis (PCA) and partial least squares regression (PLSR), which have been necessary to be able to arrive at our results. The general attitude is that glucose, at physiological levels, are below the detectable range of spectroscopes [5]. Although, an approach measuring changes in hydrogen bonds in H_2O as an indicator of glucose concentration, has given some hints that it should be possible [5].

The main results from our findings suggest that it is possible to detect glucose at physiological levels in a sample fluid, partly consisting of peritoneal fluid.

2 Theory

2.1 Diabetes mellitus and blood glucose regulation

Diabetes Mellitus Diabetes Mellitus is a metabolic disease which impairs an individuals ability to keep blood glucose (BG) levels within the normal range. Type 1 diabetes is characterized by the inability to produce insulin, it is an autoimmune disease in which the immune system attacks the body's own tissue. In particular, the β-cells located in the Islets of Langerhans in the pancreas are destroyed. This is where insulin is normally secreted from. It is believed that both genetic and viral factors are involved in type 1, although it is not yet well understood [6]. Patients with type 2 diabetes, however, either show reduced insulin secretion, or insulin resistance, or both. It is assumed that 90% of the cases of diabetes are of type 2 [7].

In healthy individuals normal BG levels will primarily stay in the range of 3.5-5.6 mmol/L (63-101 mg/dl), referred to as the euglycemic or normoglycemic range. After a meal the BG level will rise and then usually return to the normal range within 3 hours [4]. BG levels above and below normoglycemic range are referred to as hyperglycemic or hypoglycemic, respectively. The BG levels during fasting are usually examined when determining whether a patient is diabetic or not. Alternatively, when the BG levels after a carbohydrate-rich meal remains abnormally high, this indicates diabetes type 1 or 2. Patients with BG during fasting which does not decrease below 6.9 mmol/L (125 mg/dl) will be diagnosed with diabetes. Also, patients with BG levels measured to stay between 5.6 and 6.9 mmol/L (100-125 mg/dl) are referred to as having impaired fasting glucose and may be diagnosed with pre-diabetes, considered to be in danger of developing diabetes type 2 [8].

Tight regulation of blood glucose is vital to maintain normal body function. The two signalling hormones insulin and glucagon are the main part of the glucose-regulatory system. They are both secreted by the pancreas in order to maintain the glucose-insulin homeostasis [7]. Insulin are secreted by β-cells in response to high BG levels. While glucagon are secreted by α-cells in response to low BG levels.

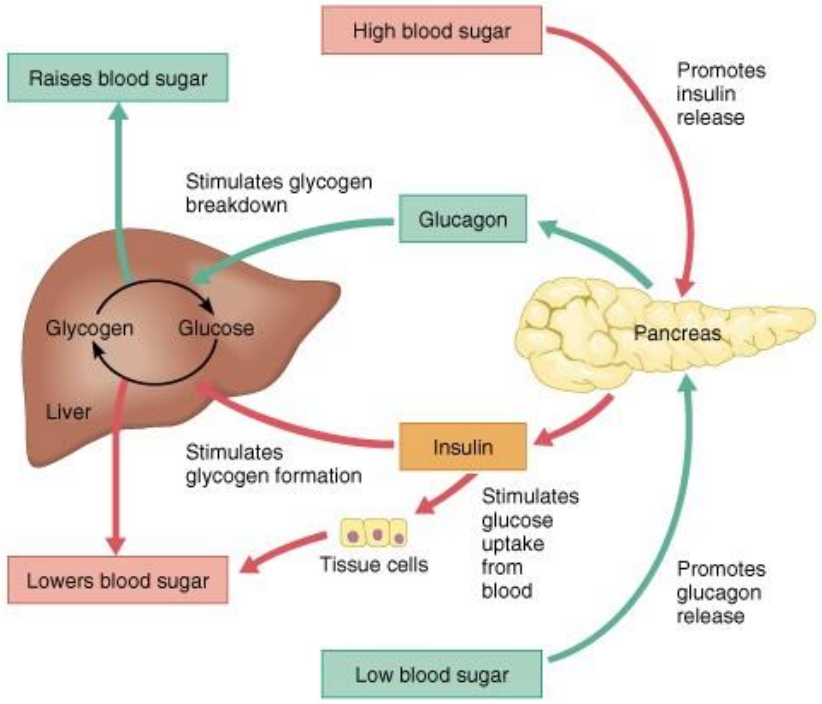

Figure 2.1: Illustration of the reciprocal effects of insulin and glucagon release

The inability to regulate BG levels to stay in the normoglycemic range leads to a series of long term complications, and, in critical cases, to coma and death. Pre-diabetes carries an increased risk of cardiovascular disease, and its treatment can result in delay or prevention of the onset of type 2 diabetes [8].

In 2000 [6] reported that the number of people with diabetes mellitus world wide was 100 million. In 2014 [1] reported an estimate of 387 million people, and that the number will increase to 592 million by 2035. Also, in every coun-

try the number of people with diabetes type 2 is increasing [1].

Today, treatment of diabetes type 1 is done on the basis of self monitoring of BG. This is done with finger-prick methods which are painful, inconvenient and does not give an accurate picture of the transient behaviour of BG levels. The development of an artificial pancreas should solve the problem of closed loop blood glucose control to achieve normoglycemia in diabetics. It is reported that any delay of more than 6 minutes in the measurement will prevent effective real-time feedback control [4].

With this background, we give a description of blood glucose sensors available today.

2.2 Blood glucose sensors

Both [4] and [9] classifies blood glucose sensors according to their invasiveness, based on the method of measurement and the placement of the sensor. Invasive devices either penetrates the skin or are completely implanted to gain direct access to interstitial fluid, peritoneal fluid or blood. Hospitalized patients are typically monitored with invasive methods, extracting blood directly from the intravenous space, and using lab instruments based on enzymatic methods for ex-vivo BG determination. Minimally invasive devices are placed outside the body, applying one of several existing fluid extraction methods to the skin to obtain small samples of blood or interstitial fluid. Noninvasive methods are devices that does not penetrate the skin, either as transdermal sensors, or to measure body fluids including saliva, breath and the aqueous humour of the eye [9].

Another classification are done with respect to the technology the sensors

are based on. The main classes are optical methods and electro-chemical methods. Here we will present the methods for glucose measurement, as covered by [4] and [9], with special attention to NIR spectroscopy. Note that the physical properties, which is the foundation for each method, could be measured with similar instrumentaion. An example is absorption and scatter change which would both be measured by a spectroscope.

2.2.1 Infrared Absorption spectroscopy

The principles of infrared absorption are described in numerous works on the basics of absorption spectroscopy, this presentation is based on [10] and [11]. Measurement of the absorption of light are one of the most used and researched methods for determination of BG in noninvasive applications [4]. Infrared absorption methods relies on the fact that bonds between atoms vibrate at different frequencies in the interaction with light. This causes light to be absorbed at specific wavelengths depending on the composition of molecules in the material being analysed. The molecular structure defines possible motions between the atoms, this gives rise to a set of degrees of freedom determining the molecule's vibrational modes. These vibrational phenomena is seen as absorption bands along the infrared spectrum. In general, a molecule with N atoms has 3N-6 modes of vibration. The basic vibrations are illustrated in figure 2.2.

The harmonic and anharmonic oscillator models are used to describe the vibrations from a mechanical perspective. In the harmonic case the model is given by two masses connected by a spring where Hooke's law gives the potential energy. Quantum mechanic treatment shows that only discrete energy levels, and only transitions between neighbouring levels are allowed. This leads to the frequency of the fundamental vibrations. Extending the harmonic case to include:

- Repulsive forces between atoms.

- Dissociation of the atomic bonds when strongly extended.

We get the anharmonic model where the energy levels are no longer equidistant as in the harmonic case. Further, it allows transitions over two or three or more energy levels, which are called the first, second, and so on, overtones. We also observe combinations of the sum and difference between different transitions.

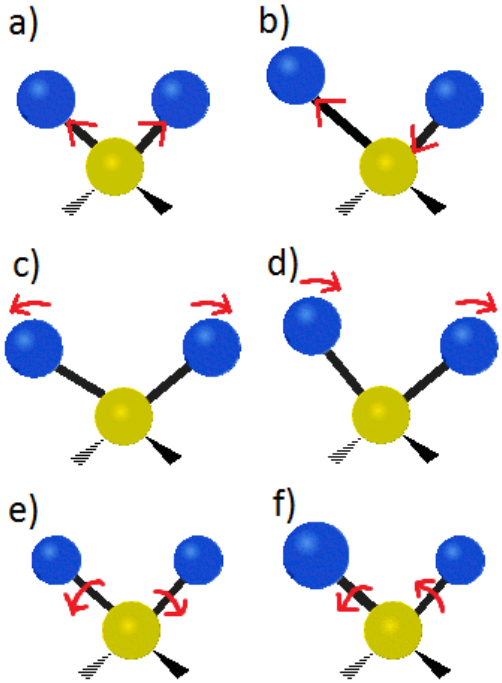

Figure 2.2: Basic vibrational modes of a molecule: a) symmetrical stretching; b) asymmetrical stretching; c) bending; d) rocking; e) wagging; f) twisting. Adapted from [12]

The Beer-Lambert law is used to relate the absorption of light to the composition of the sample. The law can be expressed in terms of transmission, T:

$$T = \frac{I}{I_0} = e^{-\varepsilon Lc} \tag{2.1}$$

as it states that there is an exponential relationship between the transmission and the product of ε, the molar extinction coefficient $[(mol/l)^{-1}cm^{-1}]$, c, the molar concentration $[mol/l]$, and L, the optical path length $[cm]$. Here I_0 is the intensity of the incident optical radiation, and I is the transmitted intensity. Measurements of absorption are usually reported in absorbance, A, defined by

$$A = -log(\frac{I}{I_0}) = \varepsilon Lc \tag{2.2}$$

such that there is a linear relationship between the absorbance and the concentration of the absorbing material. Then the total absorption in the analysed material becomes the sum of the absorbance of each species at that particular

wavelength.

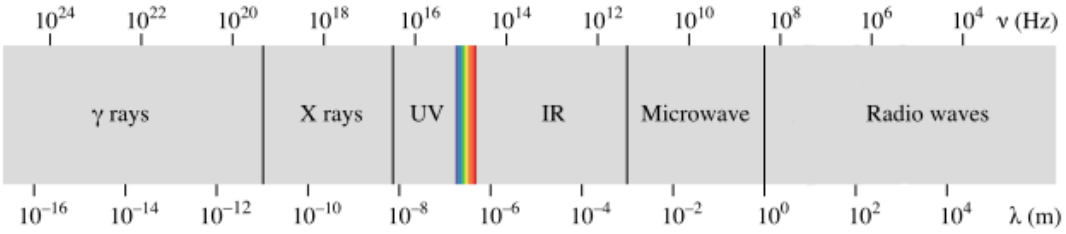

Figure 2.3: The electromagnetic spectrum and its subregions, adapted from [13]

Figure2.3 shows the electromagnetic spectrum with the classes of electromagnetic radiation. The infrared region are further divided into the near infrared (NIR), mid infrared (MIR) and the far infrared (FIR) region. Measurements of the infrared absorption spectrum is traditionally separated into the study of the NIR range and the MIR range. This is due to the vibrational phenomena observed in these ranges, and the practical technological solutions.

Generally, a spectroscope consists of a light source and a detector. The light source is used to send light at the sample, which then may interact in several ways. Some light are reflected, some are transmitted and some are scattered. A detector is set up to collect the light, often selectively for either the reflected, the transmitted or the scattered part. The combination of light source and detector technology dictates which spectral ranges can be measured.

Mid IR sensors The fundamental vibrations of molecules are found in the MIR range. This is primarily what makes the MIR region attractive for absorption spectroscopy. The range of $(500 - 2000\ cm^{-1})$ is often referred to as the fingerprint region of organic molecules. As this region is used for identification of chemicals.

MIR sensors have been studied for the use in quantitative glucose analysis. Measurements of aqueous glucose solutions and subcutaneous measurements have been performed [14; 4].

Near IR sensors In the NIR range we find overtones of the fundamental vibrations and bands caused by the combination of different vibrational modes. The specificity of NIR spectroscopy are strongly decreased in comparison with the MIR methods. This is mainly due to the overlap of these bands [10]. The observed absorption bands can also be 100 to 1000 times weaker than the fundamental bands [11].

[15] gives a list of the distinguishing characteristics of commercially available NIR instruments. These are:

Optical configuration
Scan rates
Source type
Detector type
Sample averaging technique
Dustproofing
Waterproofing
Vibration-tolerant
Optimized for transmittance/reflectance

Table 2.1: Distinguishing characteristics of NIR instrumentation

Of these characteristics, the most descriptive of the technology used in a certain instrument are source type, detector type and optical configuration. The most frequently used detectors are based on silicon, PbS and InGaAs photoconductive materials, while the most frequently used light source is a halogen-tungsten lamp [11]. The optical configuration of an instrument can be classified by whether it is based on filter (interference or Acousto-optical), LED, dispersive optics or Fourier-transform.

- Interference filters were used in the first commercially available NIR instruments [15]. Fabri-Perrot filters were used as wavelength selectors for the reflected/transmitted light. More recently acousto-optical tunable filters are used to make instruments without movable parts. They work by

letting a radio frequency signal excite a piezoelectric material which is attached to a birefringent crystal. This induces acoustic waves in the crystal which causes refraction of the light in a narrow wavelength band. The light passes through the crystal and produces two monochromatic beams. The radio frequency controls the wavelength of the output beams.

- LED based instruments uses LED as the light source. They can either produce broad, polychromatic light, or use a set of LEDs to produce narrow bands (around 30 nm bandwidth) at selected wavelengths. This is utilized as a method to make cheap and portable NIR sensors. LEDs in the range of 700-1100 nm are available at low cost, while LEDs operating at higher wavelengths are more expensive. Use of particular wavelengths instead of a broad spectra is contributing to specialize the instruments for qualitative and quantitative analyses of particular materials. Studies directed towards implantable, LED based BG sensors has been conducted [2].

- Dispersive optics can be configured as predispersive or postdispersive, depending the placement of the diffraction grating. The diffraction grating's role is to disperse the polychromatic light, break it into its constituent parts, where the spectral resolution will be determined by the size of the grating. A moving diffraction grating will either send monochromatic light through the sample (predeispersively) to the detector, or disperse the light after having passed through the sample (postdispersive). A nonmoving grating, however, is the modern alternative, it works postdispersively by sending the light onto an array of PbS and InGaAs detectors.

- Fourier-transform spectrophotometers use Michelson-interferometers. They work by letting the light from the source hit a mirror which splits it into two beams. One beam reflects off a fixed mirror while the other is reflected off a movable mirror, before they are joined and sent into the

detector. This gives an interferogram of intensities as a function of the difference in path length between the two beams. Fourier transform is then used to recover the intensities of the transmitted or reflected light as a function of wavelength.

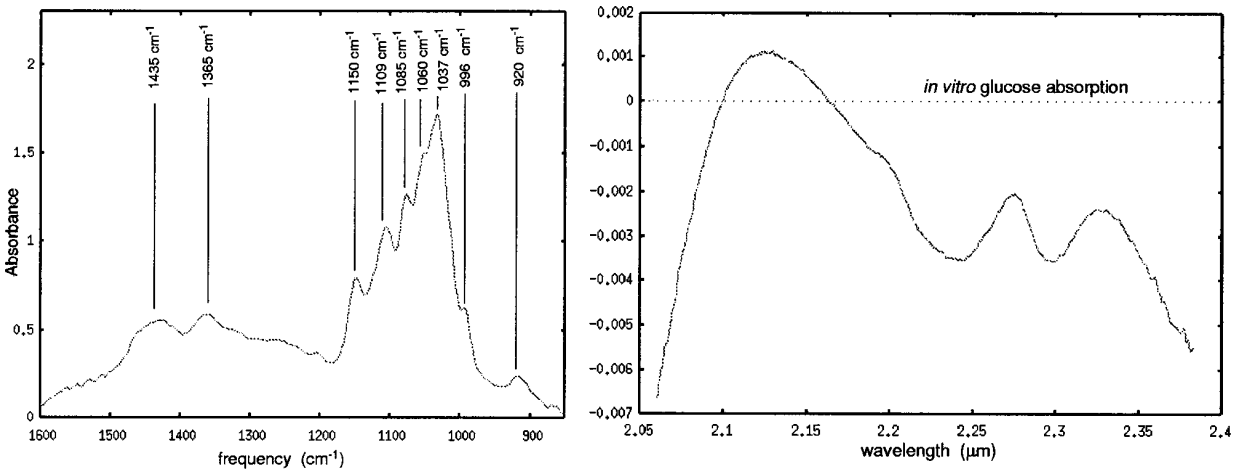

Figure 2.4: Spectra of aqueous glucose with water spectra subtracted. Figure from [6]

The two wavelength regions in the NIR band that are most commonly used in glucose measurements are the first overtone band at $1560 - 1850nm$, and the combination band at $2080 - 2325nm$ [16].

Previous NIR studies There are done numerous studies with NIR sensors in whole blood, blood plasma and artificial physiological solutions. However, at present there has not been reported any results from measurement in peritoneal fluid. A study established that glucose can be measured in blood in vitro to $\pm$ 0.83 mmol/l (15 mg/dl) using NIR sensors and mulitple wavelengths. It is not clear which wavelengths are being used in particular, but they state that they use multiple linear regression and PLS to make predictions of glucose value, pathlengths over 1 mm yielded less successful results due to poor signal to noise ratio [17]. In a subsequent study they applied an array of six diodes for

glucose determination in bovine blood samples, and got similar results [2].

2.2.2 Scatter change

Light scattering is a result of the light dispersing when interacting with scattering particles in the medium and differences in the refractive index of the substances in the medium. Increase in glucose concentration leads to grater refractive index of blood plasma and interstitial fluid. The scattering coefficient is a factor that expresses the attenuation caused by scattering:

$$\mu_s = f(\rho, a, g, \frac{n_{cell}}{c_{medium}}) \tag{2.3}$$

where ρ is the number of density of scattering cells in the observation volume, a is the diameter of the cells, g is the anisotropy factor (the average cosine of the angle at which a photon is scattered), n_{cell} is the refractive index of the cells, and n_{medium} is the refractive index of interstitial fluid. The scattering effect is calculated from measurements of diffuse reflectance, and can be achieved by a set-up similar to that of absorbance measurements.

2.2.3 Raman spectrometry

Raman scattering is one of two types of photon scattering which may occur when photons interact with molecules.

- Elastic scattering, or Rayleigh scattering, is the case when the incident photon collides with the molecule with no exchange of energy. The photon preserves its energy and frequency.

- Inelastic scattering, or Raman scattering, causes the incident photon to exchange energy with the molecule in an inelastic collision. This results in a scattered photon with a shifted frequency.

The energy difference caused by the inelastic collision is called the Raman shift:

$$E_v = E_i - E_s \tag{2.4}$$

where E_i is the energy of the incident photon, E_s is the energy of the scattered photon, and E_v is the vibrational energy of the molecule. The energy of the resulting scattered photon could be higher (called anti-Stokes shift) or lower (called Stokes shift) than that of the incident photon. The amount of photons of each energy level are counted and produces a vibrational spectra. Most photon collisions are elastic, however, and only 0.001% of the incident light are given off as Raman scattering. The resulting spectra will be independent of the excitation frequency used. One advantage of the Raman scattering method is that it is insensitive to water absorption, however, the same insensitivity applies to all measured substances due to the weak Raman signal.

2.2.4 Polarimetry

Polarimetry is based on measuring the change in polarisation observed in light passing through a solution containing an optical active material. Glucose is an optically active molecule and the amount of rotation is linearly dependent on the concentration of glucose in a solution [4]. As with absorption sensors, several factors influence the specificity of the polarimetric measurements. However, the technological solution for polarimetric sensors, make them great candidates for miniaturization [6].

2.2.5 Electrochemical

Electrochemical based methods can be categorized as enzymatic and non-enzymatic. They use an electrode with a polarizing voltage applied, and measures the current resulting from an electrochemical reaction with glucose.

Enzymatic In enzymatic approaches, a glucose specific enzyme, typically glucose oxidase (GO_X), catalyzes the oxidation of glucose to gluconolactone. In this process, the enzyme is converted to its reduced form. The redox cofactor of the enzyme is covalently bonded to the working electrode, thus facilitating the reoxidation of enzymes by direct electron transfer from the working electrode. The process is given by the following reactions:

$$Glucose \ + \ GO_X(FAD) \rightarrow Gluconolactone \ + \ GO_X(FADH_2) \tag{2.5}$$

$$GO_X(FADH_2) \xrightarrow[V]{AG/AG^+} GO_X \ + \ 2H^+ \ + \ 2e^- \tag{2.6}$$

This results in a current which can be correlated to the glucose concentration.

The ABL 725 Radiometer (which we have used for reference measurements of glucose concentration) applies a similar approach. An electrode with a multilayer membrane is used. A silver cathode, platinum anode pair is used to measure the current due to oxidation of H_2O_2. The outer membrane layer is permeable to glucose. The glucose is transported from the sample across the membrane and into an enzyme layer where it is converted to gluconic acid by:

$$Glucose \ + \ O_2 \rightarrow Gluconicacid \ + \ H_2O_2 \tag{2.7}$$

the H_2O_2 is transported across the inner membrane to the anode where it is oxidized:

$$H_2O_2 \rightarrow 2H^+ \ + O_2 \ + \ 2e^- \tag{2.8}$$

With an applied voltage, a current is produced which is proportional to the amount of H_2O_2, which again is proportional to the amount of glucose.

Other variations of enzymatic methods exists, and are described in [9].

Non-enzymatic Non-enzymatic glucose detection is based on direct electro-oxidation of glucose to gluconic acid at electrodes nanostructured to get the properties of high surface area and electrocatalytic activity. This process is described by the following reaction:

$$Glucose \xrightarrow[V]{Ag/Ag^{+}} Gluconolactone + 2H^{-} + 2e^{-} \tag{2.9}$$

The resulting current is correlated with glucose concentration.

2.2.6 Fluorescent Techniques

There are two categories of fluorescence based techniques: glucose-oxidase based and affinity binding sensors.

Sensors in the first category use the electroenzymatic oxidation of glucose by glucose-oxidase GOX! in order to generate an optically detectable glucose-dependent signal.

Fluorescent affinity-binding sensors utilize competitive binding between glucose and a suitably labeled fluorescent compound to a common receptor site.

In general, fluorescence sensors offer the advantage that can be made highly specific to glucose and eliminate many of the potential interferences common with other techniques. However, they suffer the serious drawback that in all cases exogenous chemistry is required which must be introduced to the body or sample. Additionally, the chemistry may be susceptible to degradation over time.

Other methods, including light diffraction and dielectric spectroscopy, exist and are described in [4; 9; 6].

2.2.7 Intraperitoneal glucose sensing

There are some issues that has to be explored in the development of IP glucose sensing. One is the dynamics of the IP fluid, it is not completely known how BG

levels is reflected in th IP fluid, although studies has shown strong correlation, and short time delay between BG and intraperitoneal glucose levels [3]. This is very promising for realising an artificial pancreas, based on intraperitoneal glucose sensing and insulin delivery. A system may also eventually supply glucagon to better avoid hypoglycemia.

Almost all research are investigating measurements of blood glucose either done in blood samples, both in-vivo and ex-vivo, or in interstitial fluid (ISF), both subcutaneously and transcutaneously. Therefore, these methods should be applicable to peritoneal fluid as well. This assumption is based on the fact that the composition of peritoneal fluid is similar to that of blood plasma, and contains approximately 90% water [18]. Still, the presence of confounding material as metabolites and proteins makes specific glucose sensing difficult .

One challenge with sensors placed in blood and interstitial fluid is biofouling, seen as a biofilm layer covering the implanted sensor. However, the situation may be better in the peritoneum as it is considered less immunoreactive [7]

Another advantage of peritoneal measurement given by [3], is that it is expected to be robust toward physiological fluctuations, which are a major problem with subcutaneous measurements.

It appears to be great potential in developing a glucose sensor specialised for the peritoneal cavity.

2.3 Multivariate calibration

The problem of predicting blood glucose concentration from sensor readings is called the calibration problem and is best dealt with by means of multivariate calibration techniques. Partial least squares regression (PLSR) has been widely employed in the treatment of data from NIR measurements [19]. Both principal component analysis (PCA) and partial least squares regression (PLSR) are bilin-

ear modeling methods which seeks to reduce datasets to a lesser dimensional space.

Principal component analysis is a singular value decomposition of the X covariance matrix. X in our case is the acquired spectral data, consisting of x_k samples times n measurement variables. Each principal component is found as the largest eigenvector of the covariance matrix in an iterative process. The extracted component is then subtracted from the data, and the process is repeated. Each consecutive component explains less of the observed variance in the data.

Partial least squares regression is regression based on partial least-square models. Components, the latent variables of the X data matrix, are extracted as in PCA, however, now from the explained X/Y covariance. Where Y in our case is glucose concentration. Each consecutive PC may be estimated by extracting the largest eigenvector of the remaining residual X/Y covariance matrix [20]. The relationships in the data can be found by projecting the X and Y space on low dimensional hyperplanes. The model finds the multidimensional direction in the X space that explains the maximum multidimensional variance in the Y space.

These methods are used extensively in 5. For details about multivariate analysis and in particular the PCA and PLSR methods, see [20].

3 Aim of the study

The aim of this study was to investigate the possibilities of using near infrared spectroscopic measurements to detect and quantify glucose concentration in peritoneal fluid samples. This was done with a fibre dip probe in samples obtained from patients at St. Olavs Hospital. The measurements was done by transflection in small sample volumes, hoping to shed some light the eventual future application of this method in an implantable glucose sensor. The acquired spectra were analysed with the use of the multivariate calibration techniques PCA and PLSR. Particular useful wavelengths were identified by MW-PLSR.

4 Acquisition of Spectral Data

A general procedure for data acquisition and analysis is given in [21]. The section: *how to develop and interpret a PLSR model* outlines 6 steps for a general methodology, where Step 2 is *Get good data*. Here, the design of the experimental setup will be described. This was an iterative process where the resulting measurements from one experiment were used to improve the protocol for the next experiment. The procedures are described accompanied with some comments on intermediate results. The goal was to make the measurements repeatable and accurate, by minimising the effect of confounding variables described in chapter 2.

4.1 FOSS NIRSystems 6500

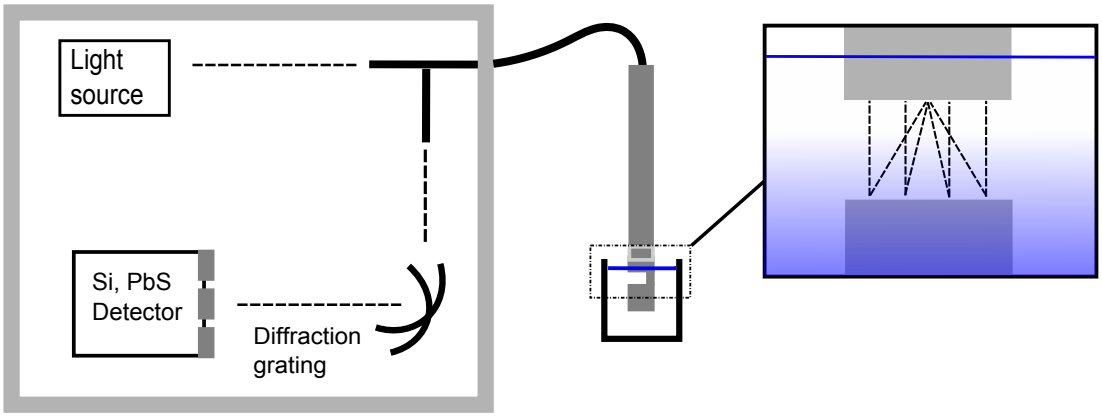

Figure 4.1: Foss 6500 with fibre optic dip probe

The spectrophotometer available for experimentation was the FOSS NIRSystems 6500 found in Bjørn Kåre Alsberg's hyperspectral imaging laboratory at the department of chemistry. The FOSS instrument uses a halogen-tungsten lamp to produce broadband light directed at the sample. The reflected light is sent through a movable diffraction grating, such that the detector scans across

the range 400 to 2500 nm. For the range 400-1100 nm, it uses a silicon detector, and in the range 1100-2500 a lead-sulfide detector.

It is equipped with a *SmartProbe Analyzer*, a multi-fibre interactance immersion dip probe which can be used for transflectance and reflectance measurements in solids, powders and liquids. We were interested in it's capability of transflectance measurement in liquids. The optical fibre is 1.5 m long and the dip probe. The output light is sent through a bundle of fibres surrounding the fibres used to collect the reflected/transflected light.

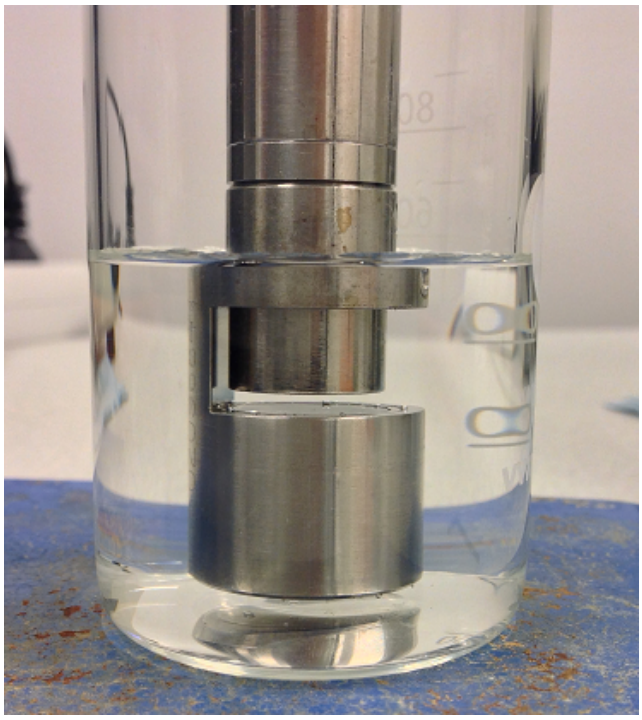

Figure 4.2: The fibre dip probe immersed in Ringer's solution in a 100 ml Griffin beaker

A mirror to reflect and focus the light is attached to the end of the probe. The optical pathlength is the length of the path that the light travels along when it goes out of the fibre, interacts with the sample and back into the fibre. In order to adjust the pathlength, spacer rings of varying thickness are placed on the probe, such that the mirror housing are shifted up or down relative to the tip of the fibre probe. The mirror is held in place by four screws. The

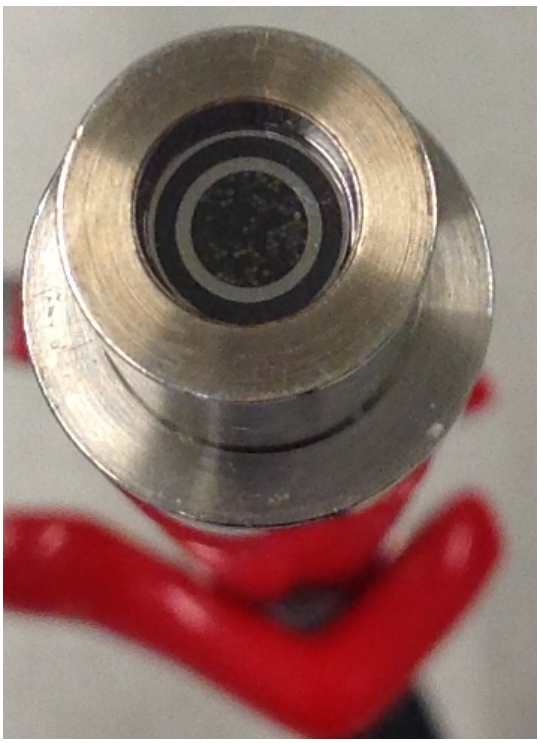

Figure 4.3: The end of the fibre dip probe. The output light is directed through the outer fibres and collected in the inner fibre bundle, separated by a metal casing.

Vision software provided by FOSS is used as interface with the spectroscope. A data collection method has to be defined, setting the instrument parameters for the data acquisition of the current operational mode. For all measurements conducted here, we have used the same data collection method, defined as "dip probe ip" shown in figure4.4

Before operation can ensue the lamp needs to warm up, and the internal temperature stabilize. This takes approximately 30 minutes. Before the instrument is stable, there are far to much noise for any data collection to be reasonable. An instrument performance test can be run to monitor the state of the instrument, and should be performed routinely. The results from this indicates the operational qualification of the instrument. In particular, it includes a test of the amount of noise over the whole spectral region. The test is "passed" if the noise are below certain user defined limits. We have used the default settings

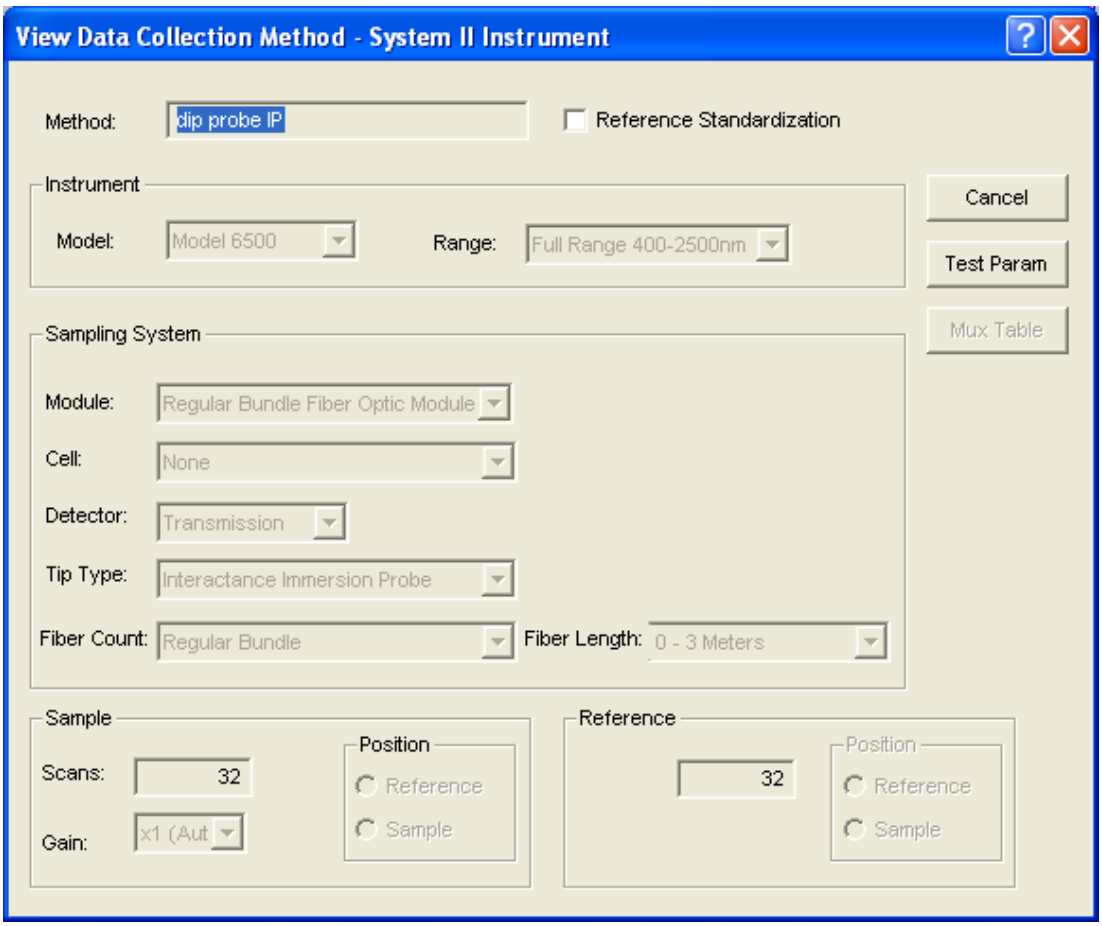

Figure 4.4: The Data Collection Method setting the parameters for data acquisition with Vision

for these limits when conducting the performance test.

4.2 Ringer's Solution and Glucose

Ringer's solution Ringer's solution is a isotonic solution with electrolyte contents similar to the interstitial fluid of the body. It is normally used in connection with intravenous therapy. The type we have used is Ringer Acetate produced by Fresenius Kabi, it was obtained from St. Olavs Hospital.

Contents	per 1000 ml
Natrium chlorid	$5.9\ g$
Natrium acetate	$4.1\ g$
Kalium chlorid	$300\ mg$
Calcium chlorid	$295\ mg$
Magnesium chlorid	$200\ mg$
Elektrolytter	$[mmol/l]$
Na^+	131
K^+	4
Ca^{2+}	2
Mg^{2+}	1
Cl^-	112
acetate	30

Table 4.1: Contents of Ringer Acetate

Glucose The glucose used is dextrose, produced by CreArome (Sweden), it contains 91% carbohydrate of which 99.5% are glucose. The remaining contents is not declared on the package and are unknown.

For the preparation of the desired sample glucose concentration, the same procedure where followed for all experiments. A lab weighing scale with precision of 0.01 g was used. A 10 ml volumetric flask was placed on the scale, and the scale reset. Glucose was carefully added until the desired weight was reached. Then water, Ringer's solution or peritoneal fluid was added up to the 10 ml mark.

4.3 Initial Experiments With FOSS 6500

The first experiments were performed as a test run of the equipment, and to gain insight of the disturbances that influenced the obtained spectral data. The very first test run were performed with water prepared with 3 different glucose concentrations and measured at different optical pathlengths. This data contained noise and disturbances which made it hard to compare the acquired spectra to each other.

The next experiment were more carefully planned and were performed with glucose in Ringer Acetate.

Sample preparation A sample of Ringer acetate with glucose concentration of $10mmol/l$ were prepared, sample G_5. We obtained a series of 4 other samples at the desired glucose concentration by diluting the G_5 sample with an appropriate amount of Ringer without added glucose.

Sample	Ringer	G_5	$[mmol/l]$
G_1	2/3	0	3.33
G_2	1/2	1/2	5
G_3	1/3	2/3	6.67
G_4	1/6	5/6	8.33
G_5	0	1	10

Table 4.2: Parts of Ringer and G_5 in each sample in the first Ringer-glucose series

The initial experiments did not give any convincing results for determining glucose concentration. Even though PLSR yielded excellent predictive capability. The main problem was that the measurements were not taken in random order, bur rather in order of increasing glucose concentration. This made it difficult to identify any useful information in the analysis due to the dominant effect of instrumental drift. Ending up with good prediction results based on the wrong phenomena is a possible pitfall when using PLSR. Great care should be taken when interpreting the given results.

4.4 Development of Experiment Protocol

An iterative process of trial and failure best describes the development of the resulting experiment protocol for the acquisition of spectral data. The goal of such a protocol is to describe and explain the performed experiment in such detail that the results can be reproduced correctly. Noise and sources of random variation in the experimental parameters had to be removed. The parameters

related to the experimental setup, not given by the contents of the sample fluid, are sought to be held constant. Some of these parameters are given by: Path-length variation, bubbles, temperature, noise and disturbances from radiating sources in the lab, variations in humidity, the position of the fibre and drift in the instrument. We tried to deal with the ones with greatest influence on the experimental setup.

4.4.1 Sample volume

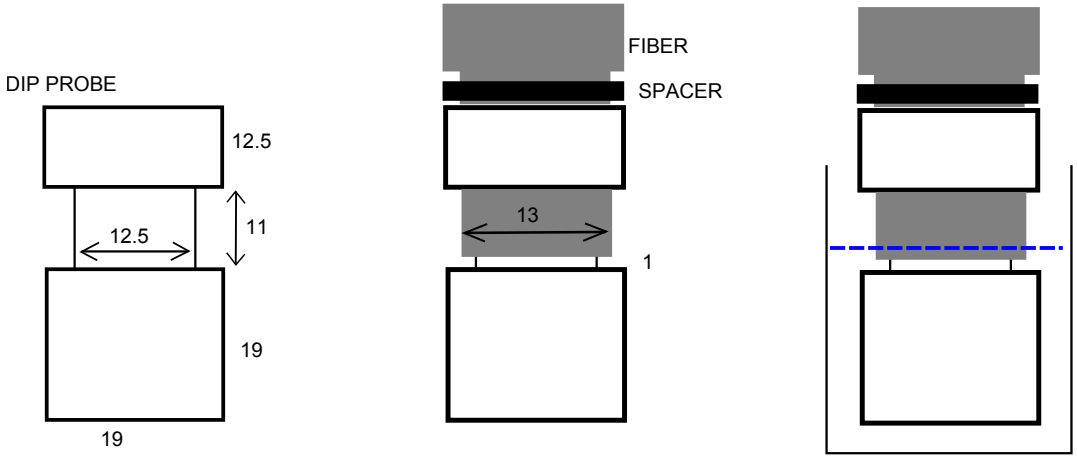

Figure 4.5: Sketch of the cell needed to perform measurements in small sample volumes. Dip probe measurements in mm.

One of the specifications in the development of an implantable sensor is the volume of the sample used for measurement. This will be given by the design of the sensor, however, in our case there was also a practical restriction by the amount of available peritoneal fluid. This lead to the need for a small as possible sample volume. Then we could also produce multiple replicates of the samples when there are enough fluid available from one patient. It was important that it would be transparent enough to allow visual inspection of the sample between the fibre tip and the mirror. The measurements needed to make a sample volume of $2\ ml$ were calculated. The sketch are seen in figure

4.5.

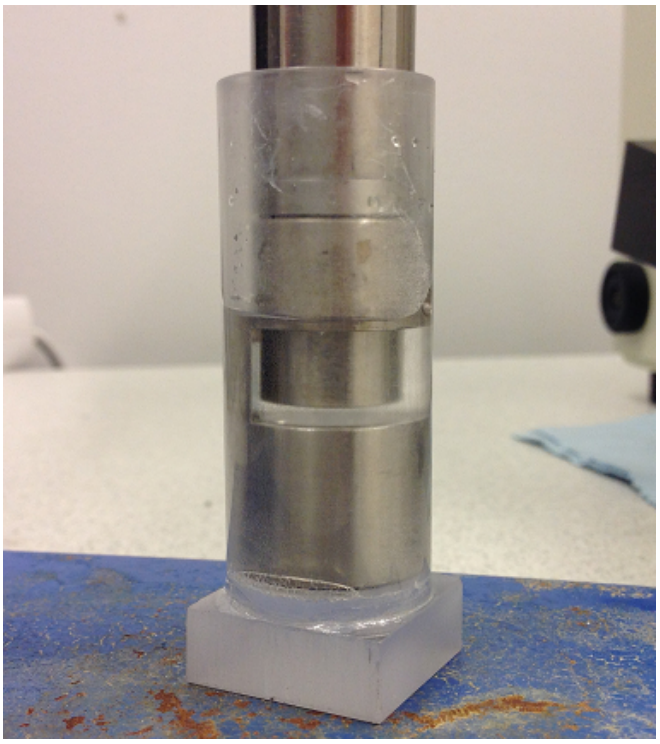

Figure 4.6: The fibre dip probe immersed in Ringer's solution in the new sample cell.

A sample cell to meet these requirements was produced in the workshop at the department of engineering cybernetics. The cell is pictured in figure4.6.

4.4.2 Temperature

To minimize the effect of temperature change on the spectra, the sample temperature needed to be controlled. We solved this in a simple way by storing the samples in a water bath with manually controlled temperature. The temperature was measured using a digital thermocouple thermometer. Both the temperature of the water in the bath and the samples were measured and monitored during the experiments. The temperature in the water bath proved to be more stable than the variations experienced when keeping the samples at room temperature in between measurements.

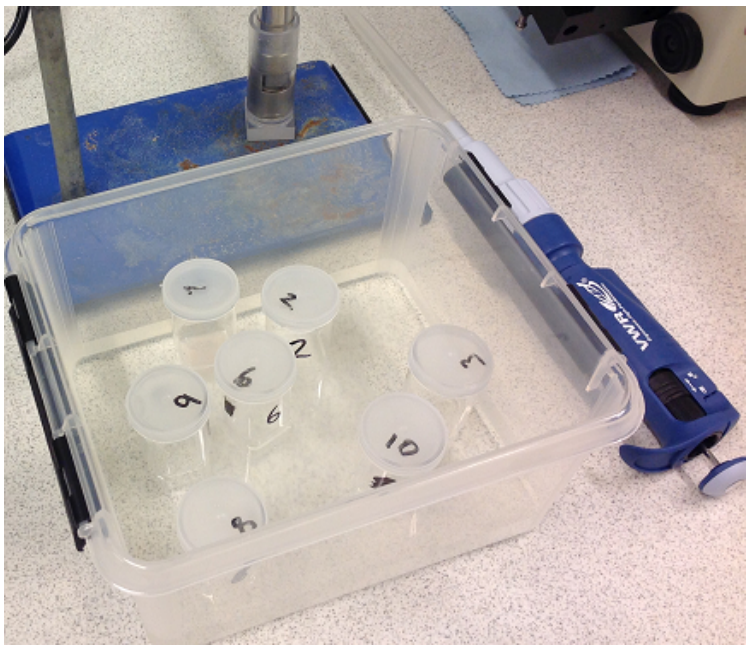

Figure 4.7: Peritoneal fluid samples kept in water during experiments. Waterbath gave stable sample temperature.

4.4.3 Bubbles

When immersing the dip probe in the sample liquid, air tended to form bubbles that would gather between the mirror and the tip of the fibre. Bubbles under a certain diameter would not cause any interference with the measurement. However, with larger bubbles of air present, the data was rendered useless, since, in reality, only the absorbance of air had been measured. When present they were easily detected by inspection of the measured spectra. In peritoneal fluid, which seemed to possess higher viscosity than water and Ringer's solution, bubbles would more easily form when the fibre probe was inserted into the sample cell. To avoid bubbles from forming, the probe had to be inserted carefully into the sample cell at an angle such that the air did not get trapped between the mirror and fibre tip. With this precaution, the problem was almost eliminated. If the effect of bubbles was detected during subsequent experiments, the probe was removed and inserted again for a new measurement.

4.4.4 Optical path length

When measuring solutions which mainly contains water, the distance should be as small as possible, to avoid saturation in the water absorption peaks. This is to maintain as much of the spectral information as possible. The pathlength were adjusted with a set of spacer rings. The thinnest of the original spacer rings from FOSS was $3.8\ mm$. The $3.8\ mm$ ring gave a gap between the mirror and fibre of $2\ mm$, and thus an optical pathlength of $4\ mm$. Two other rings found in the lab were used to obtain optical pathlengths of $2\ mm$ and $1.4\ mm$. A new ring was produced in the workshop at department of engineering cybernetics in order to achieve a pathlength of $0.4\ mm$.

Small changes in pathlength leads to disturbances in the acquired spectra. It is not hard to see the significant difference between the three spectra from peritoneal fluid samples in figure4.8, although they are all measured at a pathlength of $0.4\ mm$. This difference would be expected as the result from a change in pathlength, according to Beer-Lambert's law (equation 2.2). The observation that the difference seems consistent along the whole spectrum tells us that it is not a phenomenon related to specific wavelengths.

4.4.5 Disturbances in path length

The effect of variation in pathlength on the acquired spectra during repeated measurements is not too hard to identify, and should in theory neither be hard to correct for. However, it represents another unknown parameter in the calibration, and if it is possible to avoid this variation, we would prefer to keep it out of the equation. It can also be difficult to distinguish variation on pathlength from bias caused by instrumental drift. After the initial experiments it became obvious that it was difficult to keep the pathlength constant. Taking reference measurements, wiping the mirror, tightening the screws and relocating the fibre were all operations which seemed to introduce slight changes in

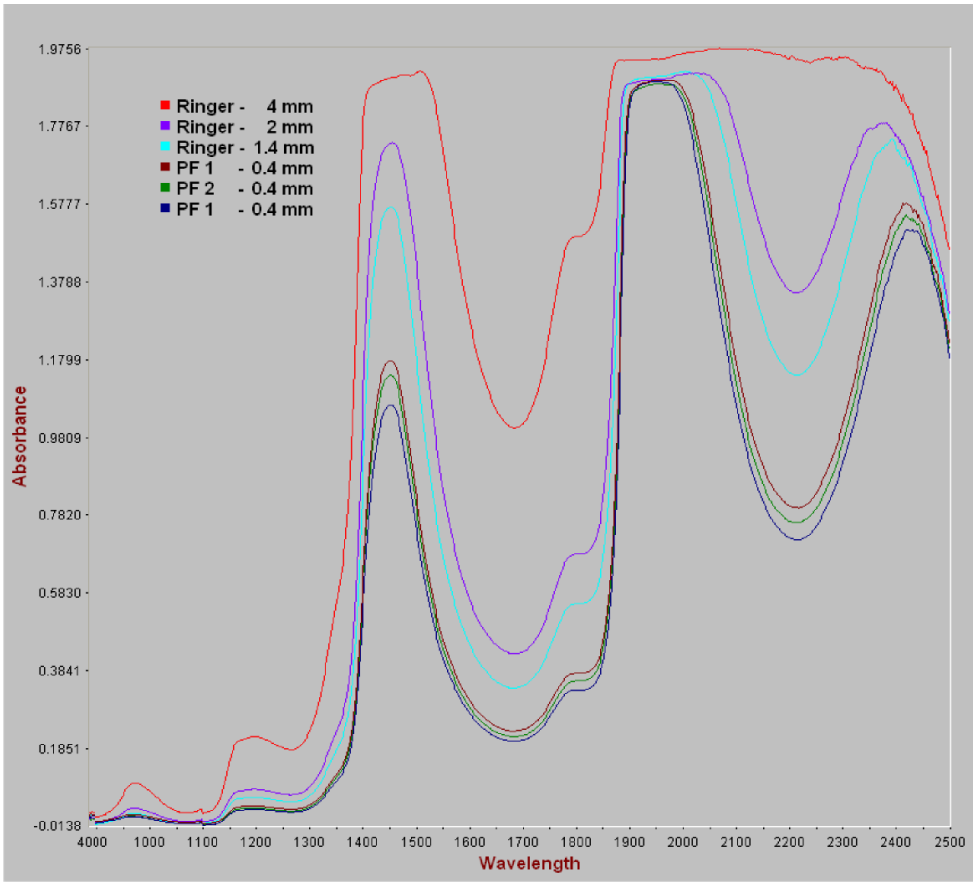

Figure 4.8: Absorbance spectra collected using different sized spacer rings giving different optical pathlength. Although the same spacer ring is used for acquisition of the PF (peritoneal fluid) spectra, shifts in the spectra are clearly visible.

the optical pathlength. Seemingly, the spectra randomly jumped up and down between measurements.

Great improvement were seen when we fastened the dip probe with a clamp to a supporting stand. Then we could hold the dip probe in the same position, also minimizing movement of the fibre. We also cleaned the mirror between measurements, without removing the mirror from the fibre. This meant not having to tighten and loose the screws. An operation which could change the position of the mirror.

The final experimental protocol was used for subequent measuremnts.

4.5 Experiment Protocol: Glucose in peritoneal fluid

Objective: Obtain spectral data of peritoneal fluid with varying glucose concentration in the physiological range. The data should be suitable for detection and quantification of glucose.

Method: A series of different glucose concentrations are mixed from peritoneal fluid samples obtained from St. Olavs Hospital. Glucose is added to one half of the sample volume to a concentration of $10\ mmol/l$, this is sample G_5. The volume of each sample in the series should be minimum $2\ ml$.

Concentration of mixed series

Sample	Peritoneal Fluid	G_4	$[mmol/l]$
G_1	1	0	0
G_2	0.75	0.25	2.5
G_3	0.50	0.50	5
G_4	0.25	0.75	7.5
G_5	0	1	10

- One series is made from each patient. Depending on the amount of peritoneal fluid, a number of replicates are made. The concentration levels are adjusted to the original glucose concentration and the amount of fluid.
- Vision is used to run "Instrument Performance Test" before the experiment can start.
- "Wavelength Linearization" is performed each day the experiment is running.

- Reference is set in the instrument in an empty sample cell before each series of measurement. Spectrum of distilled water is also acquired.

Measurements

- Measurement is done with interactance immersion dip probe attached to FOSS NIRSystems 6500.
- The sample is placed in a custom $2\ ml$ sample cell.
- Sample temperature is controlled with a waterbath.
- Optical pathlength is set with a $2\ mm$ spacer ring, leaving the gap between mirror and fibre at $0.2\ mm$, and the pathlength at $0.4\ mm$.
- The dip probe are held by a clamp in a support stand to avoid unnecessary movement and disturbance in the fibre-mirror assembly.
- The samples are measured in random order, generated by the python function `shuffle`.

Data The Acquired spectral data are exported from Vision to Excel.

	Glucose	time	Replicate #	...	Spectral data ...
Measured sample 1					
Measured sample 2					

Table 4.3: Data exported from Vision software

Material: Peritoneal fluid samples, Ringer Acetate, FOSS NIRSystems 6500 photospectrometer equipped with interactance immersion dip probe, Vision software, weighing scale (precision 0.01g), thermocouple thermometer, glucose powder.

4.6 Temperature Effect

Temperature has a large and evident effect on the water spectra. This is well known, and correction for this effect is needed in order to observe the effect of varying glucose. One experiment were conducted were we had cooled the samples prior to measurement and then let the samples heat back to room temperature. We recorded temperatures from 10 to 25 C . In another experiment we had heated the samples and then let them cool in room temperature. Recorded temperature range of 38 to 23 C. We used the thermocouple for measuring the temperature and kept the samples in water bath for more stable temperature change.

4.7 High Glucose Concentration

Using the protocol we conducted experiments on Ringer's solution with high glucose concentration. A sample of Ringer Acetate were prepared having a glucose concentration of 278 mmol/L (5000 mg/dl). Four samples of lower concentration were made by adding Ringer until desired glucose concentration were reached. Thus we got a series of samples at 6 concentrations: The measurements were taken before the spacer ring for $0.4\ mm$ optical pathlength was available, and were performed at an otpical pathlength of $2\ mm$.

Sample	G0	G1	G2	G3	G4	G5
Concentration [mmol/L]	0	56	111	167	222	278

Table 4.4: Samples with high glucose concentration

4.8 Blood Gas Analyzer

Radiometer ABL 725 is the blood gas analyzer used at the animal laboratory at St Olav's Hospital. The method for glucose concentration determination is de-

scribed in chapter 2 under electrochemical methods. The precision of the ABL 725 analyzer has been determined through performance testing as described in [22]. Where it is reported that the measured value of a sample will deviate from the true value by a maximum of $\pm 2S_X$. WhereS_X is the standard deviation given when considering uncertainty of bias on a random instrument for a single measurement. While S_0 is the standard deviation given for repeated measurements within a short interval of time. We used a heparinized syringe to draw fluid from the samples, which then where placed in the analyzer for extraction. 195μl of sample was drawn from the syringe. The reported standard deviations for this mode of measuring are given in table 4.5.

Glucose level	S_0	S_X
2	0.10	0.18
5	0.10	0.24
15	0.40	0.65

Table 4.5: Standard deviations for measurements on ABL725

The peritoneal fluid samples we measured had glucose levels in the upper end of the measuring range and beyond. Also, the lowest measured values were still in the upper physiological range. The measuring ranges of glucose and lactate in the ABL 725 are given in table 4.6.

	Unit	Measuring range	Reference range
Glucose	mmol/l	0.0 - 24.9 25 - 60	3.9 - 5.8 in arterial blood
Lactate	mmol/l	0.10	0.5 - 2.2 in venous blood

Table 4.6: Measuring ranges for glucose and lactate on the ABL 725, from [22]

4.9 Peritoneal Fluid Samples 1

The first peritoneal fluid samples acquired where mixed into a series. But later dismissed due to the fact that they had fermented. This was seen from mea-

surements at ABL 725, were the glucose concentration were low and the lactate values high. A sure sign of fermentation. No further analysis were taken

4.10 Peritoneal Fluid Samples 2

ABL The blood gas measurements gave important findings: The lactate concentration in the samples from patient 4 were out of the physiological reference range. They were measured to between 15 and 16 mmol/l. While the reference range is 0.5-2.2 mmol/l. Also the glucose concentrations were measured to between 46 to 54 mmol/l. Therefore the samples from patient 4 were excluded from future analysis.

Preparation 2 The samples where extracted from four patients at St. Olavs Hospital. The samples were mixed into a series of increasing glucose concentration. We knew, from the previous samples, that the glucose concentration could be higher than normal values or even outside the range we were interested in. We added glucose to one half of the fluid from each patient and mixed them to the desired glucose concentration. The plan for mixing the sample series was based on the available volume of peritoneal fluid and the amount needed to be measured three times on Foss 6500, Raman, FTIR, XDS and ABL725. Minimum 2ml for Foss 6500 (with some small consumption for each measurement, 0.3 ml for FTIR, 0.7 for Raman, 1 ml for XDS and 0.02 ml for ABL).

4.10.1 Measurements conducted at NOFIMA

We got the opportunity to measure the samples at NOFIMA, and their facilities located at Ås. The goal was to see if other methods could give complementary spectral information. Especially, FTIR and Raman measurements should ne insensitive to the high absorption of water. Also using the next generation NIR spectrometer to investigate what spectral information is "missed" with a

transflectance fibre dip probe setup when compared to regular transmission measurement.

4.10.2 Metrohm XDS

Metrohm XDS analyzer is the next generation of the FOSS 6500 spectrophotometer. We used a rapid liquid module. The samples was put in quartz cuvettes with 1 mm path length placed in the automatic sample handler. Each sample was measured three times in different cuvettes. 32 consecutive scans was taken, and averaged to minimize noise, over the full range of the instrument of 400-2500 nm. The spectral data are recorded with a resolution of 0.5 nm. The optical bandwidth of the instrument is 8.75 nm.

4.10.3 Raman Spectrometer

For the Raman measurements a LabRam HR 800 Raman microscope from Horiba Scientific (France) was used. The HR 800 is an integrated Raman system comprising a microscope coupled confocally to an 800 nm focal length spectrograph equipped with four switchable gratings. The microscope is an open BX41 confocal microscope equipped with standard objectives (10x, 50x, and 100x, a long distance 50 x objective and a macro 40 mm objective). The instrument only provides punctual analysis, and no line scanning or duo-scan imaging is possible. The instrument is equipped with an air cooled Deep Depleted CCD detector (1024 x 256 pixels), and two lasers (one internal HeNe laser and one external 785 nm diode laser). We used the HeNe laser at 632.8 nm. The peritoneal samples were pipetted into quartz cuvettes. Placed in the laser beam optics.

4.10.4 FTIR

The samples were transferred directly, in triplicate, to well plates (384 wells) in $10\mu L$ droplets, and dried in a vacuum desiccator with silica gel at room

temperature for 24 hours. FT-IR measurements were performed using a high-throughput instrument (eXTension, HTS-XT with Tensor 27 Spectrophotometer, Bruker Optik GmbH, Germany). The instrument was equipped with a deuterated L-alanine doped tri-glycine sulfate (DLaTGS) detector. Spectra were recorded in transmission mode in the spectral region from 4000 to 400 cm-1 with a resolution of 4 cm-1 Background spectra of an empty sample well were collected before each measurement of the samples to account for variation in water vapor and carbon dioxide.

5 Analysis of Spectral Data

We have used The Unscrambler X software from CAMO, to perform most of the PLSR, EMSC and outlier detection on the data sets. We have made some plots and scripts in MATLAB R2014b. The MWPLSR procedure is implemented in `MWPLSR.mat` and the EGA plots are generated by `parkes.m`

The general methodology and procedure for analysis of spectral data are described in [21; 20], special attention are also given to NIR spectral data in [20].

5.1 Preprocessing of Raw Data

In the multivariate calibration terminology, preprocessing refers to the processing of the raw data before regression and prediction is done. The goal of preprocessing is to remove noise from the data. This can be achieved by filtering high frequency noise and using EMSC which is a method for removing the effect of light scattering and other disturbances. Another approach is to take advantage of a priori knowledge about disturbances and interferences and incorporate them in the modelling process, one way to do this is described in [23].

5.1.1 Extended Multiplicative Scatter Correction

Multiplicative scatter correction (MSC) and extended MSC (EMSC), are used to remove noise due to light scattering effects. The presentation of the EMSC method given here is taken from [24]. EMSC aims to separate absorption from additive, multiplicative, and wavelength dependent effects of uncontrolled light scattering variations. Theoretically, for a solution of J absorbing constituents, Beer-Lambert's law gives the absorbance spectrum, for sample i as a linear combination of the contributions from each of the absorbing constituents:

$$\mathbf{z}_{i,chem} = c_{i,1}\mathbf{k'}_1 + ... + c_{i,j}\mathbf{k'}_j + ... + c_{i,J}\mathbf{k'}_J \tag{5.1}$$

where $c_{i,j}$ is the concentration, and $\mathbf{k}_j$ is the absorptivity spectrum of the jth constituent. For ideal conditions, with fixed optical pathlength, the measured spectrum for sample i, is $\mathbf{z}_i \approx \mathbf{z}_{i,chem}$. To approximate the physical effects related to light scattering, the measured spectra is modelled as a scaled version of the ideal spectra. The EMSC model is given as:

$$\mathbf{z}_i \approx a_i + b_i\mathbf{z}_{i,chem} + d_i\lambda + e_i\lambda^{\mathbf{2}} \tag{5.2}$$

where the coefficients a and b represents the baseline offset and the path length, respectively, relative to a reference spectrum. Coefficients d and e represents unknown, smoothly wavelength dependent spectral variations between samples. The EMSC method in Unscrambler calculates estimates of these coefficients and apply the EMSC correction to remove the baseline and pathlength variations and the wavelength dependent effects. The corrected spectra are given as:

$$\mathbf{z}_{i,corrected} = (\mathbf{z}_i - a_i - d_i\lambda - e_i\lambda^2)/b_i \tag{5.3}$$

This corrected spectra represents the chemical absorbance information found from the measured spectra: $\mathbf{z}_{i,corrected} \approx \mathbf{z}_{i,chem}$

5.1.2 Derivative analysis

Derivatives are usually investigated in the search of structural information regarding the material under investigation. Also taking the second derivative will remove baseline shifts and trends from spectra. Similar to the noise removal of EMSC. The resulting spectra, however, does not at all look similar. A problem with derivatives is that it introduces additional noise to the spectra. By taking the derivative of a noisy signal you get more noise. With our measurements, we

already are at the limit of acceptable SNR for glucose detection, so this should not yield to much information. This is what we see from attempts at doing PLSR at the derivative of the spectra. The only useful results of PLS regression on derivative spectra come from the measurements of the samples with high glucose concentration.

5.2 Wavelength Selection

Theoretically and under ideal conditions, adding spectral channels will always improve the calibration models. However, these ideal conditions and assumptions are shown to be hard to achieve in real experiments, and therefore, removing wavelengths that introduce noise to the calibration models will improve the prediction performance [25; 26]. Generally the focus should be on the wavelength regions between the water peaks. Where glucose has relatively high absorption [2; 5].

5.2.1 Moving Window Partial Least-Squares

The method of moving window partial least-squares is described in [25]. It is the procedure of applying PLSR to a window of the spectra of a certain size. By moving the window along the spectrum and computing the corresponding sum of squares of the residuals (SSR), we can get a picture of which wavelengths that holds the most information. With this information we can also avoid the parts of the spectra that contributes to uncertainty in the predictions. Thus, it is an algorithm for selecting the spectral channels with least uncertainty. The SSR are calculated at each point for prediction using 1 to A factors. This gives us SSR as function of wavelength for A calibration models.

5.3 Validation

Cross validation We have used cross-validation to asses the models predictive ability on new data, and to find the optimal number of components used in the model. When the amount of available data is limited, the cross-validation approach has been shown to give better results than dividing the data into calibration and test sets [27]. We can also see to what degree the model is under-fitted or over-fitted when comparing the mean square error of prediction (MSEP) with the cross-validated mean square error (MSECV). And choose the optimal number of components as the number which yields the lowest cross-validated prediction error.

Calibration and Test Set We have used measurements from 2 of the patients as a training set for the calibration model. The measurements from the last patient is used as new unknown input data for the calibration model to perform regression on. Results from both methods of validation are presented

5.4 EGA

Error grid analysis is used to examine the accuracy of the results in a clinical setting. In an error grid, the blood glucose values predicted from the measurements from the method under investigation are plotted against the reference values, acquired from measurements on an instrument assumed to hold higher accuracy and used as a "gold standard". The plot is divided into zones which classifies how wrong the estimated values are. Then, perfectly predicted values will lie along the diagonal, and the size of the prediction error determines which zone the plotted value falls into. These zones vary with the glucose level, because an erroneous estimate and the corresponding clinical action will have different consequences depending on the real blood glucose value. As an example, doing nothing in an hypoglycemic event is worse than if the blood glucose

is slightly elevated, in the case where the measured value shows normoglycemic conditions.

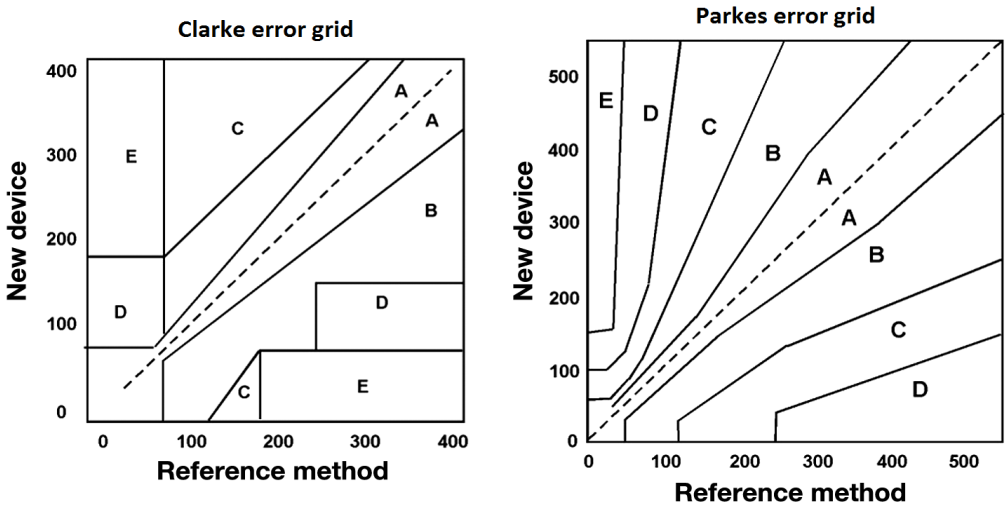

Figure 5.1: Comparison of the Parkes and Clarke error grid, adapted from [9]

Zone	Associated risk
A	Clinically accurate measurements, no effect on clinical action
B	Altered clinical action, little or no effect on clinical outcome
C	Altered clinical action, likely to affect clinical outcome
D	Altered clinical action, could have significant clinical risk
E	Altered clinical action, could have dangerous consequences

Table 5.1: Risk categories in Parkes error grid

The Clarke error grid has been widely used to assess the risk and accuracy of new measurement devices. However, a major disadvantage with Clarke's error grid is that the zone boundaries are not connected sequentially, which means that a small change in the measured glucose value may move the value from zone A (correct measurement) to zone D (potentially dangerous, failure to detect hypo or hyperglycemia), or vice versa [9]. Parkes' grid [28] consists of sequential boundaries, where an increase in the error will have to pass through the zones, indicating the increased risk in using the measured value. Both Clarke's and Parkes' grids are originally developed for evaluation of self monitoring blood glucose devices. Currently there are no consensus on the criteria to

be used for evaluation of continuous glucose monitoring devices [9]. Here we use Parkes' grid as an indication of the performance of the predicted blood glucose levels. The plots are created with *parkes.m* (a modified version of *clarke.m*, from), the risk zones and their limits were found in [29]. The risk categories are defined in table 5.1. A histogram of the distribution of the data points with respect to the zones are often given together with the plot, as a measure of the accuracy of the investigated method.

5.5 Procedure for Analysis of Measurements

The steps in the analysis are similar for all data across experiments and measuring methods.

1. **Remove bad data**

   Generally, the first step is to remove obvious faulty measurements from the spectral data. This could be due to bubbles or other foreign elements which has disturbed the measurement process. This can be seen as an empty spectra (recorded absorbance near zero for the whole spectrum), or spectra which deviates significantly in shape from what is expected.

2. **Noise and Smoothing**

   Next the data is smoothed, we have mainly used a moving average filter. This can be justified by the fact that the spectral resolution generally is higher than the bandwidth of the instrument. Also, vibrational phenomena, particularly in the NIR region, has broad absorbance peaks. Smoothing the data should then remove some of the high frequency noise without removing important spectral information. EMSC is also part of removing noise, in the form of scattering (and similar) effects.

3. **PCA**

   PCA can yield information about the data, X, and design variables, Y, that

impacts the data set in unwanted or unexpected ways. We can often gain insight to how known disturbances as scattering or temperature influences the data.

4. **PLSR**
   Finally we assess the ability to predict glucose levels in the data set by PLSR. This is done in several rounds, to remove outliers which has not been evident earlier, to compare spectral regions, and to validate.

With this as a general guide, the analysis of the experimental data was performed as described in the next sections.

5.6 NIRS 6500

The results of the initial, temperature and high glucose concentration experiments are presented here, as they contribute to the analysis of the peritoneal fluid experiments. The results of the peritoneal fluid experiments are given in chapter 6

5.6.1 Noise

As we can see from figure 5.2, there are significantly more noise in the upper and lower end of the spectrum than in the middle part. Therefore it will be advantageous to omit these wavelengths in the following analysis and calibration. The noise is caused by the scattering in the fibre, and in the optical configuration generally, as well as white noise along the whole spectrum. We know that Prediktor's GlukoPred employs a detector with range 900-2000, so we will focus our analyses on this range. This range would also be a good choice if only taking the noise characteristic into consideration. We can see fluctuations up to around $850 - 900\ nm$, and an gradual increase in intensity from around $1900\ nm$.

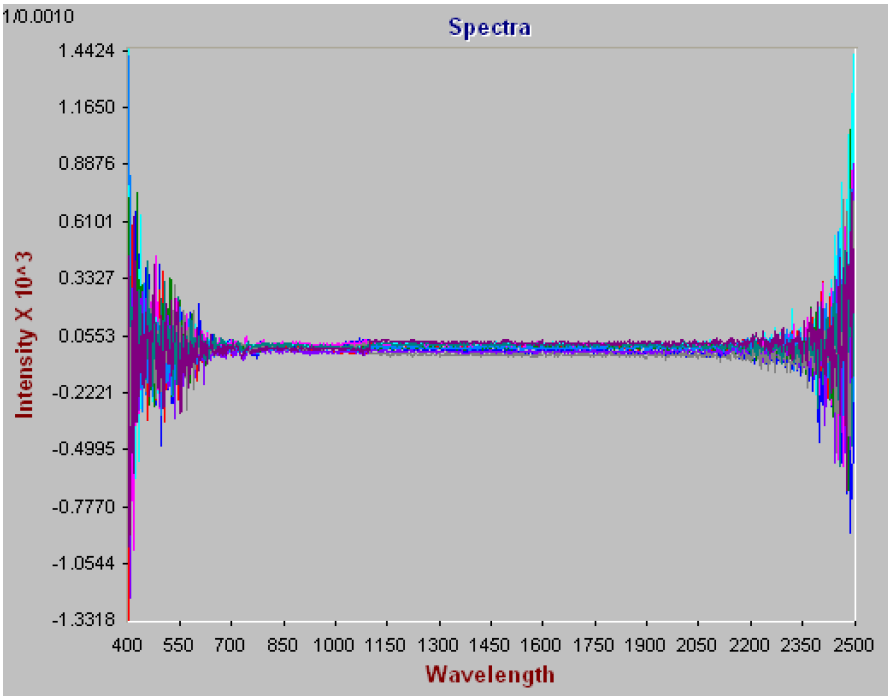

Figure 5.2: Spectrum of the noise given by Instrument Performance Test

5.6.2 Initial Glucose Experiment

Although the experiment were conducted before the protocol was finished, we ended up with a set of good data. This data will serve as an example analysis while exposing a potential pitfall regarding interpretation of PLSR models.

5.6.3 Temperature Effect

From the loadings and scores of PLSR performed on the temperature data we will try to identify the parts of the spectrum which are most sensitive to temperature change. When we later find glucose specific wavelengths we can compare them to the findings of this experiment. If the glucose wavelengths correspond poorly to temperature effect, the predictions will be more robust to temperature change.

We perform PLSR on the spectral data from the heating experiment.

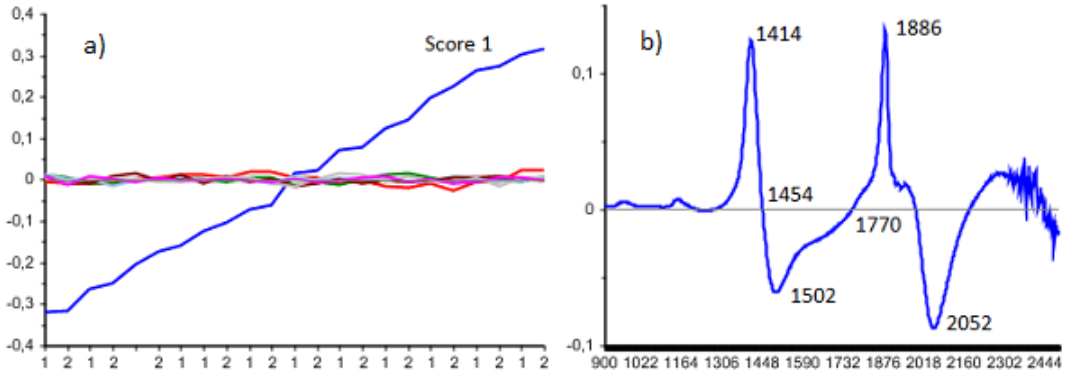

Figure 5.3: a) Scores against samples of increasing temperature. b) Factor 1 in the range 900-2498 nm.

For the cooling experiment we got the following scores and factor 1:

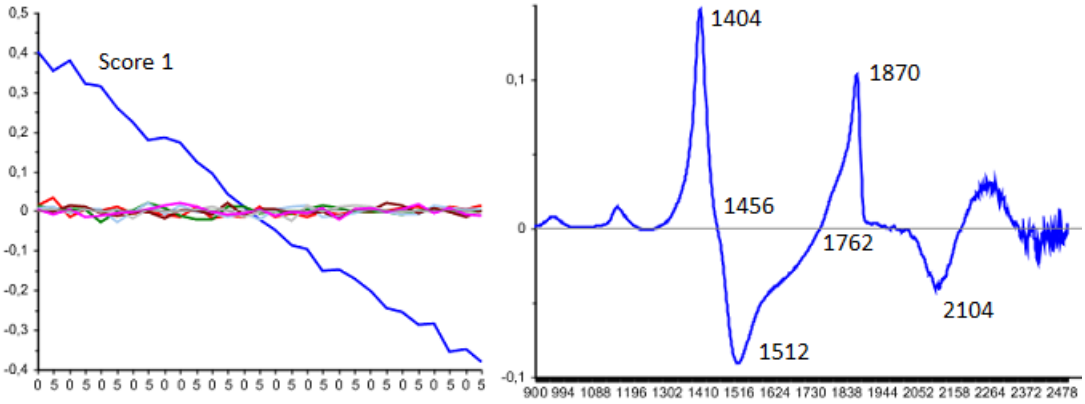

Figure 5.4: a) Scores plotted against samples of decreasing temperature. b) Factor 1 in the range 900-2498 nm.

The first factor gives an explained Y-variance of 99%. The cross-validated prediction values give:

	Heating:	**Cooling:**
R^2	0.99	0.99
RMSE	0.35	0.42
Explained Variance	99%	99%

Table 5.2: Statistics for prediction of temperature.

The wavelengths most sensitive for temperature variations are the ones just below and over the water peaks. At the water peak itself, there are a stationary (in the sense that it's absorbance does not change with temperature) point. The overtones at 950 and 1150 are also seen in the plot of factor 1.

There sensitivity seems to be somewhat lower in the range between the waterpeaks at 1450 and 1900. Which also seems to be the case between 950 and 1150. The temperature experiment, has a weakness in that the decrease and increase in temperature are correlated with eventual instrumental drift.

5.6.4 High glucose concentration

The high glucose concentration experiment has samples with glucose in the range $0 - 278\ mmol/l$ $(0 - 5000\ mg/dl)$.

Sample:	0	1	2	3	4	5
Glucose [mmol/l]	0	56	111	167	222	278

Table 5.3: Glucose concentrations in the samples of the high concentration experiment.

All data seemed good from visual inspection of the spectra. We used moving average smoothing, gap: 5. And subtracted the mean spectrum from all spectra. This is shown in figure 5.5, and it is easy to distinguish the samples from each other. The differences seen in the spectra are the ranges where variation in glucose affects the spectra.

When the differences are so easily seen, prediction can be done without the use of PLSR. However, the results are interesting for future reference. We can see that the peaks at 1402 and 1870 correspond with the peaks in the temperature loadings. This is problematic. In the region from 1400 and up, we see a great correspondence between glucose concentration and the measured absorbance, except from the range neighbouring 1480. In these experiments the temperature variation is $0.6°C$. It seems that this variation is not great enough to cause considerable problems, at these glucose levels at least.

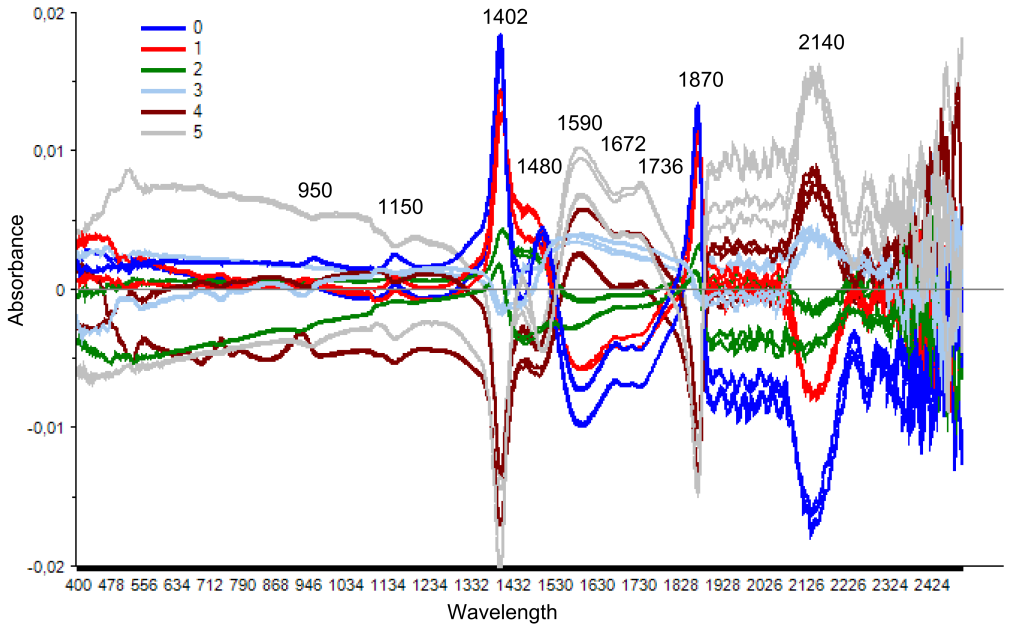

Figure 5.5: Mean centered spectra of samples 0 to 5. The differences between high and low concentration are clearly visible.

The range between 1480 and 1870 are also of great interest, in these wavelengths water absorption is at a relative minimum, while glucose absorption has a broad peak. Although influenced by noise the peak at 2140 indicates a good region to distinguish glucose levels. Since these measurements are taken at 2

From figure 5.6a, we can see that scores of factor 1 alone can distinguish the glucose levels in the respective samples. In figure 5.6b, we have the correlation loadings for factor 1 and 2. This tells us to which degree each variable contributes to the loading. The variables placed between the inner and outer ellipses are the ones which contribute to a significant extent. Blue dots are X-variables and red dots are Y-variables. The Y variable *order*, represents the order the samples where measured in.

We clearly see that it does not contribute to factor 1, while *temperature* might contribute in a minor way. We have also seen that the temperature sensitive

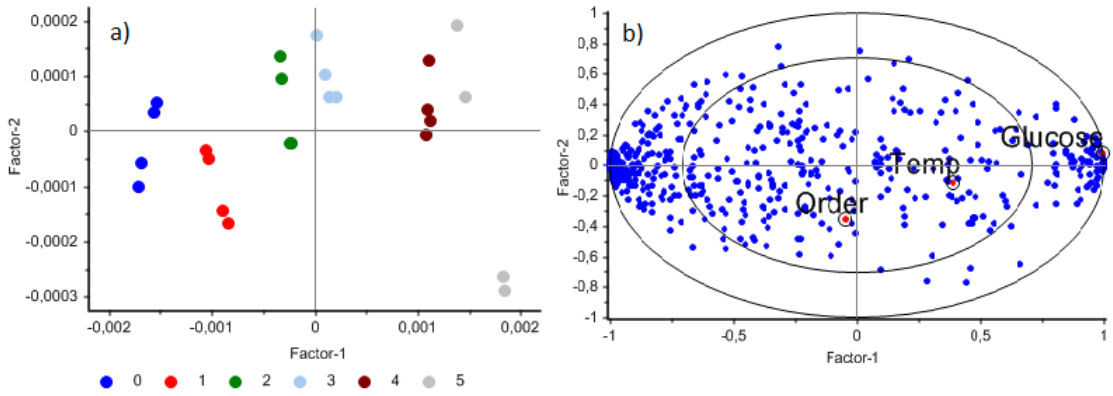

Figure 5.6: Results from PLSR on high concentration data, a) Score of factor 1 and 2. b) Correlation loadings of factor 1 and 2. Variables in the outer ellipse contribute significantly to the corresponding loading.

variables overlap with the variables responsible for the observed glucose variation. We believe this overlap also is the reason for the small correlation between factor 1 and the temperature.

The excellent prediction of high glucose concentrations can be seen from the PLSR model based on the smoothed, mean-centered data also pretreated with EMSC in the range $900 - 2000$, shown in figure 5.7. Figure 5.7a shows the predicted glucose values using only factor 1 with RMSE of $237\ mg/dl$ or 4.7%. Neither temperature (figure 5.7b) or measurement order (figure 5.7c) can be predicted, even when using 3 factors. We can also see from figure 5.8, that factor 1 clearly represents the difference in glucose concentration, as observed in figure 5.5.

5.6.5 Peritoneal fluid samples

The measurements of the first three samples in the experiment, sample 1, 27 and 18 was removed from the dataset due to high sample temperature measured by the thermocouple. With the samples removed the variation in sample temperature during the experiment was $0.6°C$.

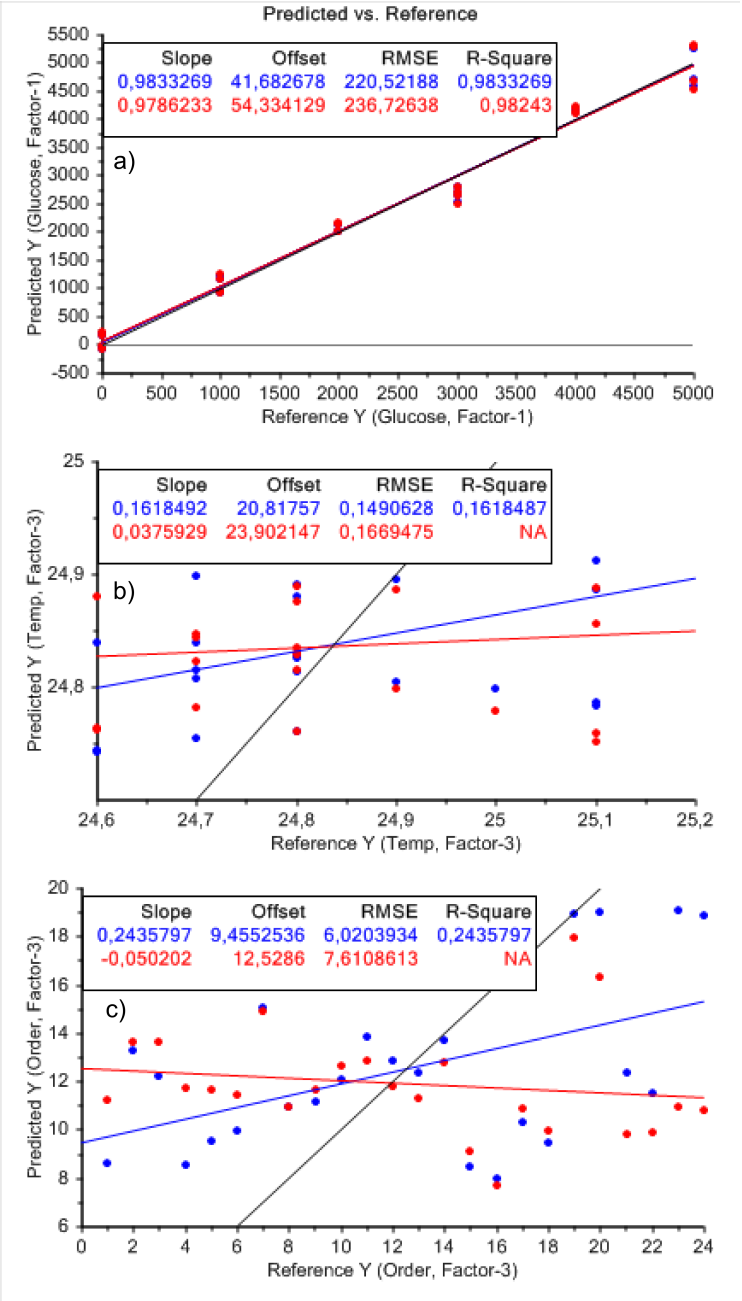

Figure 5.7: a) predicted glucose concentrations using factor 1, units in mg/dl. b) prediction of temperature using factors 1 - 3, c) prediction of order of measurement using factors 1-3.

Preprocessing 1 We first pretreated the measurements by applying moving average smoothing with segment size 9 on all spectra. Then we applied EMSC

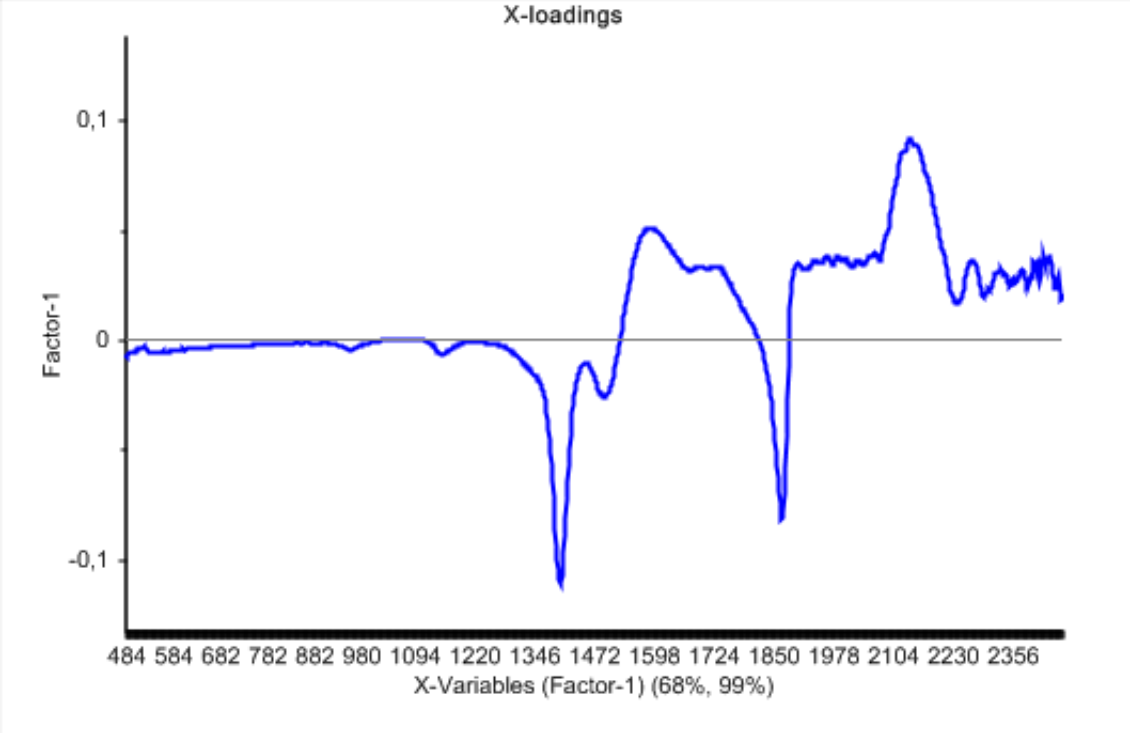

Figure 5.8: Factor 1 obtained of PLSR model of high glucose concentration.

on the measurements of patients 1 - 3 in the range 900-2100 nm.

We performed the MWPLSR procedure on the pretreated and the raw data, for measurements from patients 1 - 3. The result are seen in figure 5.10. The raw and the smoothed data appear to give similar results. There are two prominent "dips" in the residual value. These are found to be at $1350 - 1460\ nm$ and $1490 - 1620\ nm$. There are also two small features at $1730\ nm$ and $1850\ nm$. We note that the SSR values in the $1600 - 2100\ nm$ range does not reflect the observed importance of this range in the high concentration experiment. Therefore, we will include the wavelengths around the two small features as well, to see if they can contribute to the prediction. There are also consistently lower SSR in all cases at $2042\ nm$. This may be related to the effect observed at $2140\ nm$ in the high concentration experiment. However, the comparison may not hold due to the amount of noise at these wavelengths in the former ex-

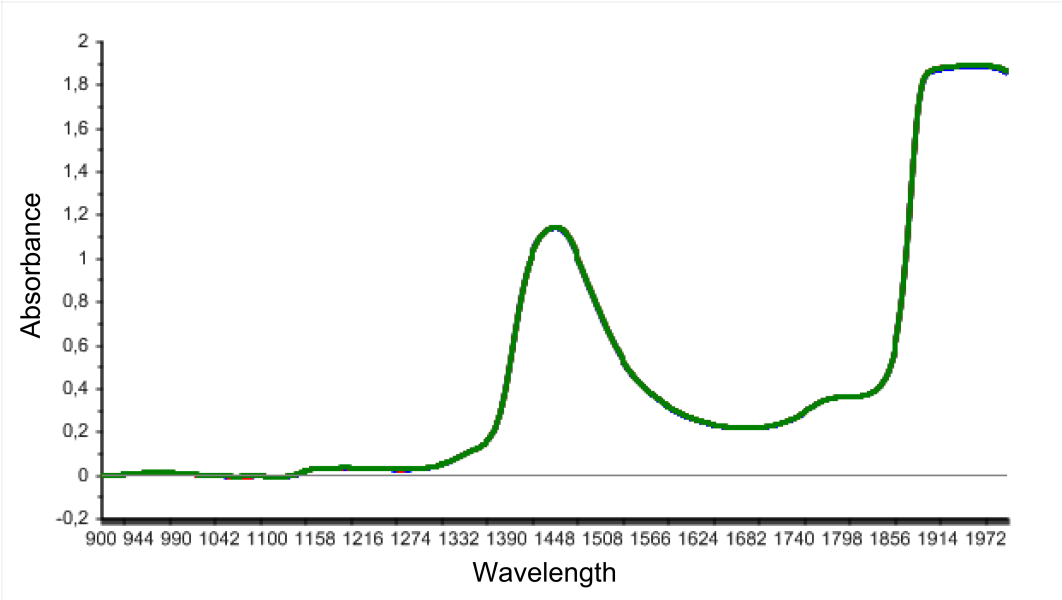

Figure 5.9: Three spectra acquired from patient 1,2 and 3, respectively, plotted together. They are almost indistinguishable by visual inspection.

periment. It still represent an interesting region. The window size used for the MWPLSR is 30 channels, or 60 nm. We choose the following set of wavelengths, MW1: $1350 - 1460$, $1490 - 1650$, $1720 - 1860$ and $2010 - 2070$ nm.

The residual lines of the data after EMSC, exhibits other characteristics. There are multiple narrow bands that are candidates for inclusion in a new set of wavelengths. Now we select single wavelengths rather than bands. We have chosen the wavelengths, P1: $978,\ 1162,\ 1378,\ 1428,\ 1512,\ 1558,\ 1620,\ 1672,\ 1744$ and 1840 nm.

Preprocessing 2 Another way to preprocess the spectra are by performing EMSC in the region 900-2100 nm, but now for the measurements of one patient at a time. This could be helpful in removing intereference specific to that patient.

Since the measurements were taken in two repeated series. We could also leave one series out to minimize the effect of instrument drift and bias. This

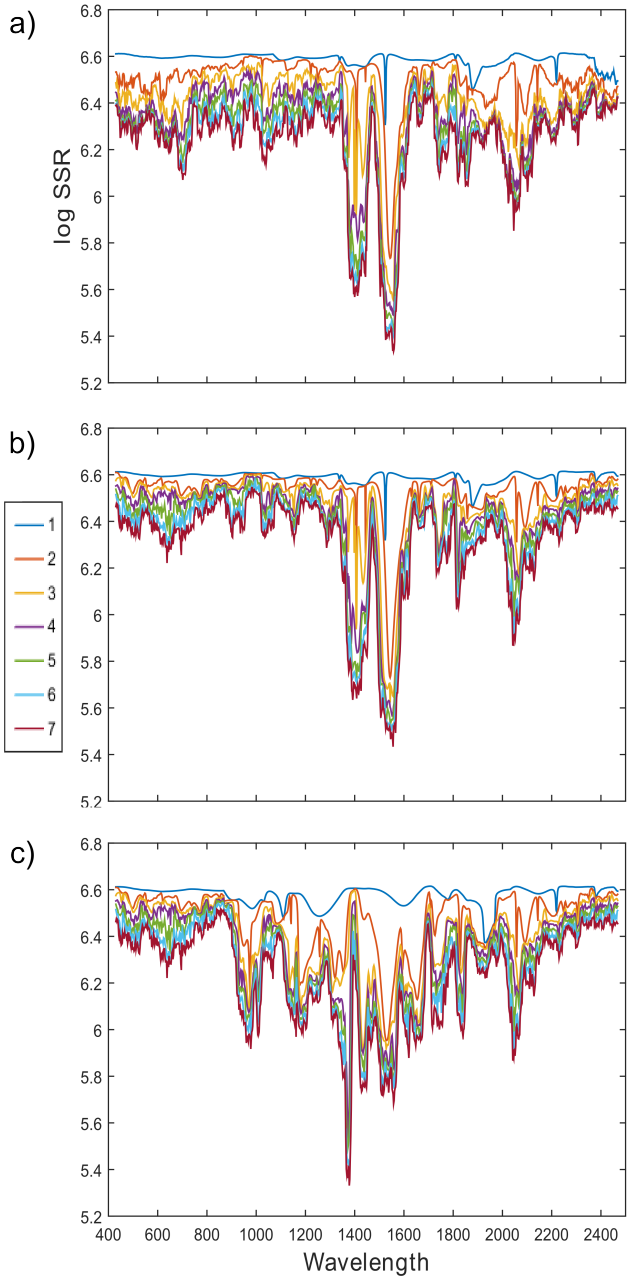

Figure 5.10: Mowing Window Partial Least Squares Regression procedure, wavelength in nm along the ordinate and logarithm of the sum of square of residuals (SSR) on the abscissa. MWPLSR applied to: a) raw data; b) after moving average; c) after moving average and EMSC on the range 900 - 2000 nm. Each line represents a number of factors used in the model calibration.

leaves a lot of possible combinations for the interpretation of the models. We summarise these calibration models by looking at the cross-validated explained Y-variance. This can be seen in figure 5.11.

Ideally, we would like to see a few factors explain close to 100% of the variance. From these plots we can see which factors contributes the most to explain the original data. If many factors contribute by a small amount each, they are most likely to represent random noise picked up in the PLSR correlation analysis, and we end up with an overfitted system. Figure 5.11,i) and l) looks most promising. These represent EMSC performed at each patient, using the P1 set of wavelengths and using both measurement series and only series 2, respectively. It is interesting that we seemingly get the best Y-variance explanation by P1.

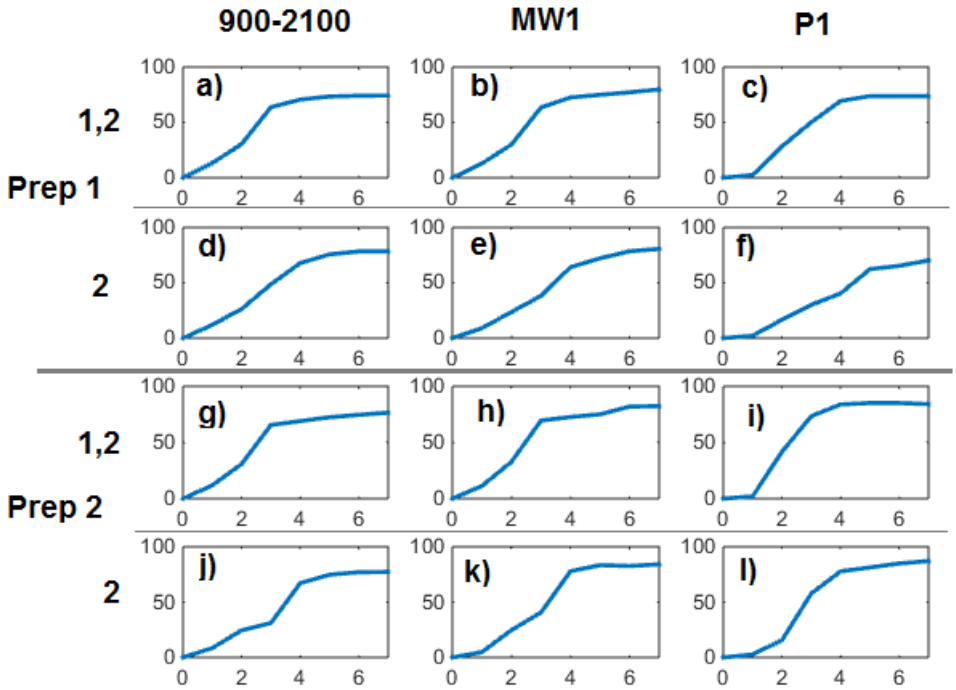

Figure 5.11: The explained Y-variance for each generated model is plotted against the number of factors used. These models are generated by using preprocessing 1 or 2 (EMSC on all measurements or separately on patients). Using the range 900-2100 nm, MW1 or P1. And by either using measurements from both series or only series 2.

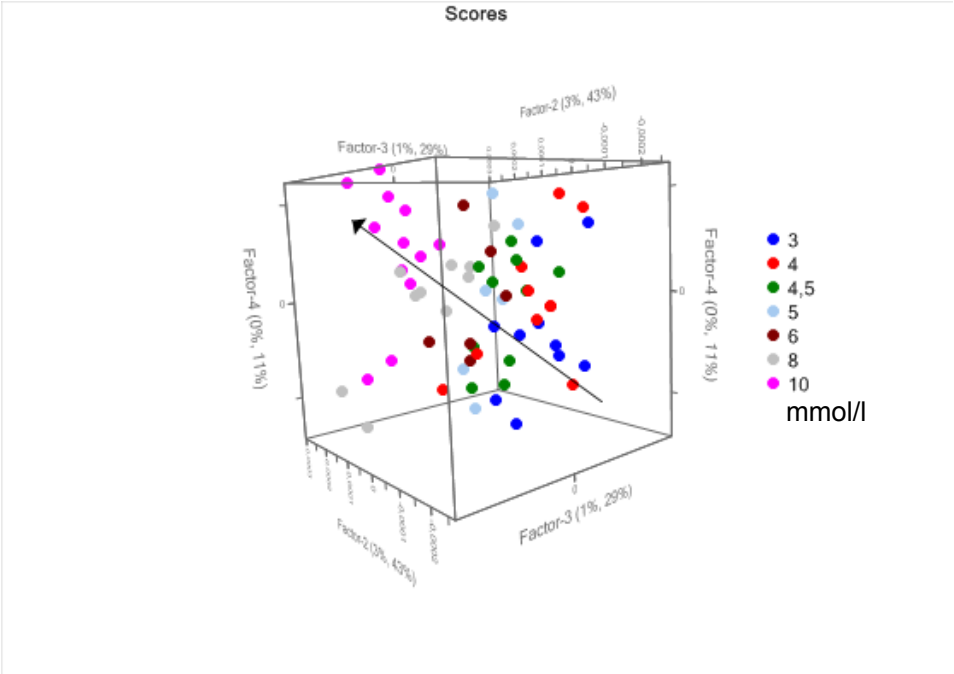

Figure 5.12: Factor 2,3 and 4, the arrow indicates the direction of increasing glucose in the factor space.

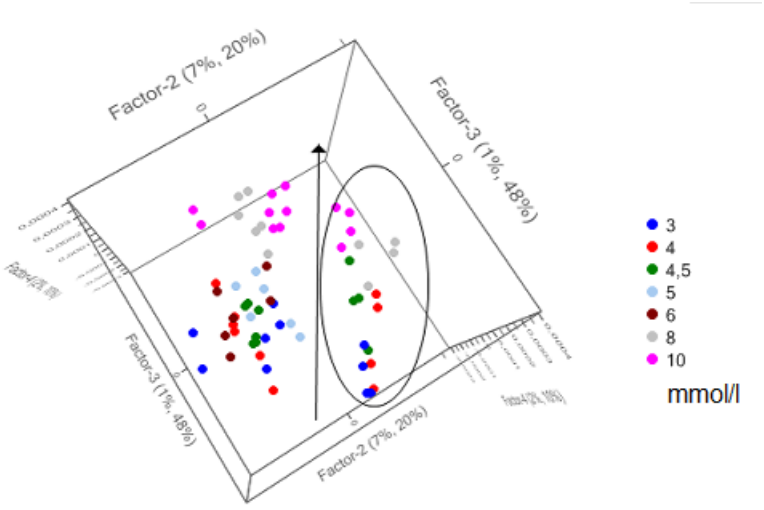

Figure 5.13: Factor 2,3 and 4, the arrow indicates direction of increasing glucose in the factor space. While the ellipse marks the measured samples from patient 2.

From inspection of factors 2,3 and 4 in a 3D scatter plot, it seems the 3 factors can be sufficient to explain the Y-variance. Also, in the case of the model

in figure 5.11,l) (factors in figure 5.13) the EMSC of each patient has helped in making the model able to separate the measurements of patient 1 from those of patient 2 and 3. The predicted glucose values are given in section 6.

Training and Test

We can use two patients as a training set while using the last as a test for calibration. This can be done in 3 ways.

	Training set	Test set
T1	2,3	1
T2	1,3	2
T3	1,2	3

Table 5.4: Patients used for test set and training set.

For this we will use measurements from both series, preprocessing 2, and the P1 wavelengths as this gave best results in the previous cross-validated models. When comparing the performance of model *i* and *l*. We may look at

model	RMSECV	R^2
i	0.96	0.85
l	0.89	0.87

Table 5.5: The cross validated root mean square error, and R^2 coefficient are used for comparison of model i) and l).

the values given in table 5.5. From this we may conclude that *l* is best based on the lower RMSE. However when comparing the explained Y-variance curves in figure 5.11, we can see that there is only one factor not contributing in the start. Whereas model *l* has two factors not contributing, but with higher explained X-variance. Also the optimal number of factors, represented by the maximum of the Y-variance curve, are lower, which indicates that we have found more useful factors. The predicted values from the training and test sets are given in section 6. We can see from figure 5.14, that there are problems in the validated test sets.

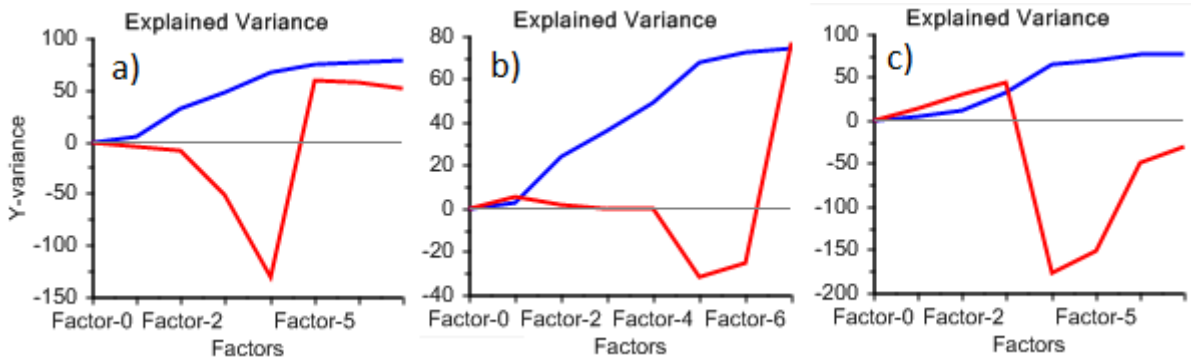

Figure 5.14: Plot of explained variance in test and training sets

5.7 Metrohm XDS

Remove spectra of samples 25-1, 26-2 and all replicates of 30 from analysis. 25-1 was due to a bubble in the sample during measurement. 26-2 and 30 was other obvious anomalies, and was removed.

We start by conducting an MWPLSR on preporcessed data. As with the FOSS measurements we use moving average smoothing here with gap 5, followed by EMSC on the whole spectrum. Then we try to identify useful wavelengths from the residual lines from the MWPLSR script.

We can see from figure 5.15 that we get another picture from the XDS instrument than the FOSS instrument. There are more information found in the upper part of the spectrum. In particular at 2112 nm and at 2275 nm, these two wavelengths promise to yield the most information, according to the MWPLSR. Moving downwards we find the water peak at 1950 nm as the noisiest part of the spectrum. As with the FOSS analysis, we try to choose the set of wavelengths which contributes most to the prediction. We choose the set of ranges as: $930 - 970$, $1255 - 1300$, $1380 - 1425$, $1555 - 1600$, $1660 - 1750$, $1790 - 1820$, $2080 - 2120$, and $2255 - 2295$ nm. For a set of specific wavelengths, we choose the nine that are marked in the figure, and in addition 1505 nm. We investigate the predictive ability of these sets of wavelengths, together with the range

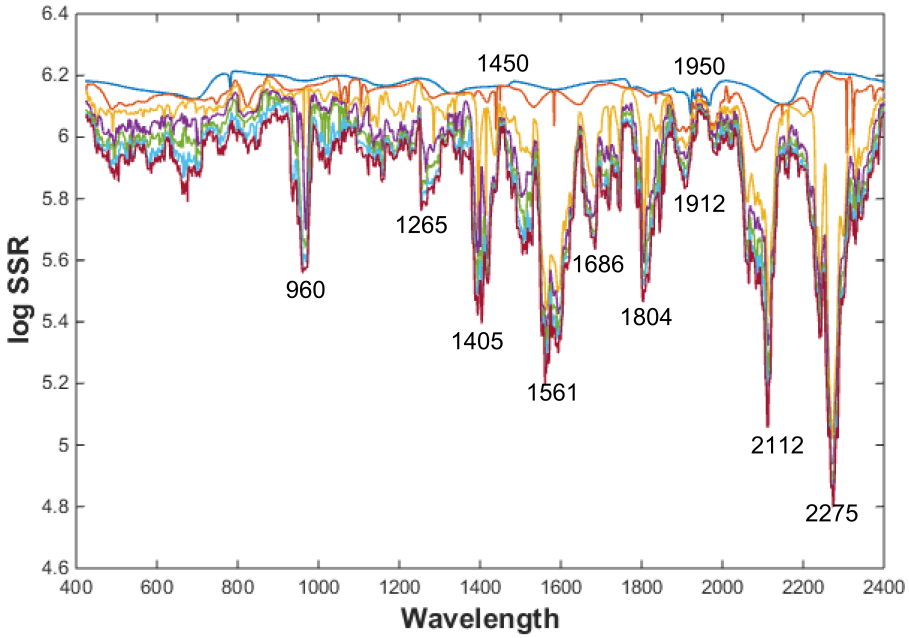

Figure 5.15: MWPLSR applied to XDS data.

$900 - 2000\ nm$.

Adjusting for Cuvette The absorption added to the measurement due to the quartz glass cuvettes was found to interfere with the analysis of the data. There were three different cuvettes with three distinct cuvette spectra. We assume that the spectra of the sample fluid measured in cuvette 2 and 3 are the same as that measured in cuvette 1. That is, the difference between the spectra obtained from each sample in the three cuvettes, are due to the differnce in the quartz cuvettes, instrument drift and random noise. We then get the measurements in cuvette 1 as:

$$\mathbf{S_1} = \mathbf{R_1} + \mathbf{1} \cdot \mathbf{k_1^T} + \mathbf{v} \tag{5.4}$$

The absorption spectra of the empty cuvette nr. 1 was measured and then subtracted from all measurements taken in that cuvette.

$$\mathbf{R_1} = \mathbf{S_1} - \mathbf{1} \cdot \mathbf{k_1^T} \tag{5.5}$$

Where $\mathbf{R_1}$ represents the spectra of the sample fluid alone, $\mathbf{S_1}$ are the measured spectra, and $\mathbf{k_1}$ is the mean of two measurments of the empty quartz cuvette. In order to estimate the cuvette part of the spectra, we subtract $\mathbf{R_1}$ from $\mathbf{S_2}$ and $\mathbf{S_3}$ to get the estimates of $\mathbf{k_2}$ and $\mathbf{k_3}$, respectively. The estimates of $\mathbf{k_2}$ and $\mathbf{k_3}$ are smoothed and subtracted from $\mathbf{S_2}$ and $\mathbf{S_3}$, such that the remaining $\mathbf{R_2}$ and $\mathbf{R_3}$ is an estimate of the measurements with some noise. We note that this does not yield the true results, but are done anyway to see what improvements can be achieved by removing known interferences from the spectra.

Preprocessing We have used moving average smoothing with gap size 9 and applied EMSC correction on the whole range.

Model	Explained Y-variance % var	RMSE	$R2$
PREP 900-2000	-64	2,4	0.01
PREP MW	83	0.97	0.83
PREP P	70	1,3	0.7
CR 900-2000	-30	2,45	NA
CR MW	83,4	0.98	0.83
CR P	76.9	1,18	0.77

Table 5.6: Stats for XDS test, PREP is preprocessin by moving average smoothing and EMSC correction on all spectra. CR has in addition the cuvette spectra subtracted. MW and P is the wavelengths found from MWPLSR

The predicted values are given in section 6. We found that the best results are achieved when we are restricting the calibration to within measurements from one patient. It is seen to have a great impact on the prediction results, when we examine the spectra from patient 3 in figure 5.16.

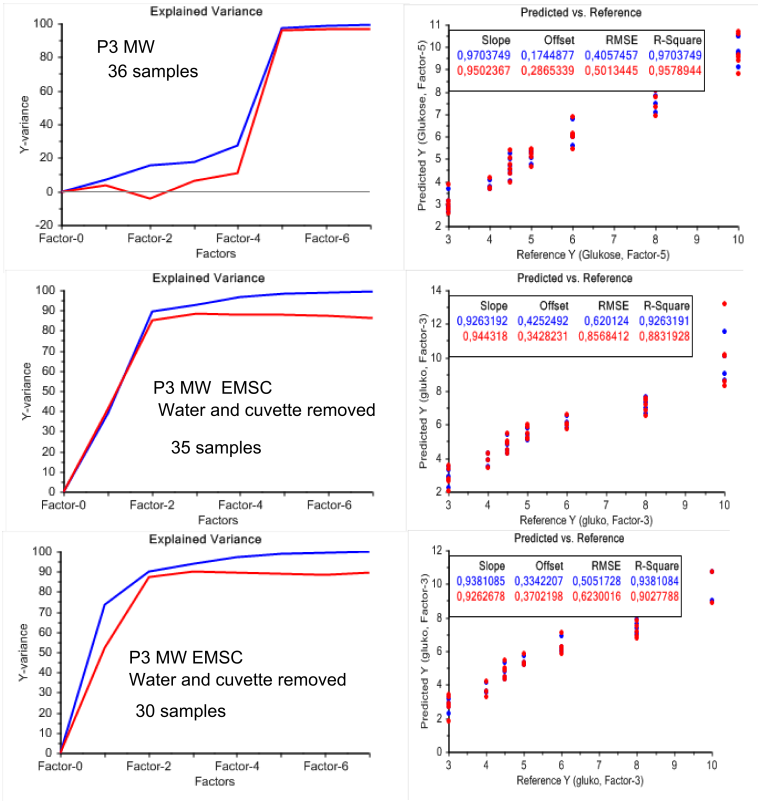

Figure 5.16: Improving the predictive ability by removing noise and outliers

5.8 Raman

We have used the same procedure for preprocessing the data as with the NIR results. First we remove the spectra acquired from sample $20-3$. Then we perfrom smoothing by moving average, gap size 11, and performed EMSC correction on the whole spectrum.

Overview of the results are given in 5.17

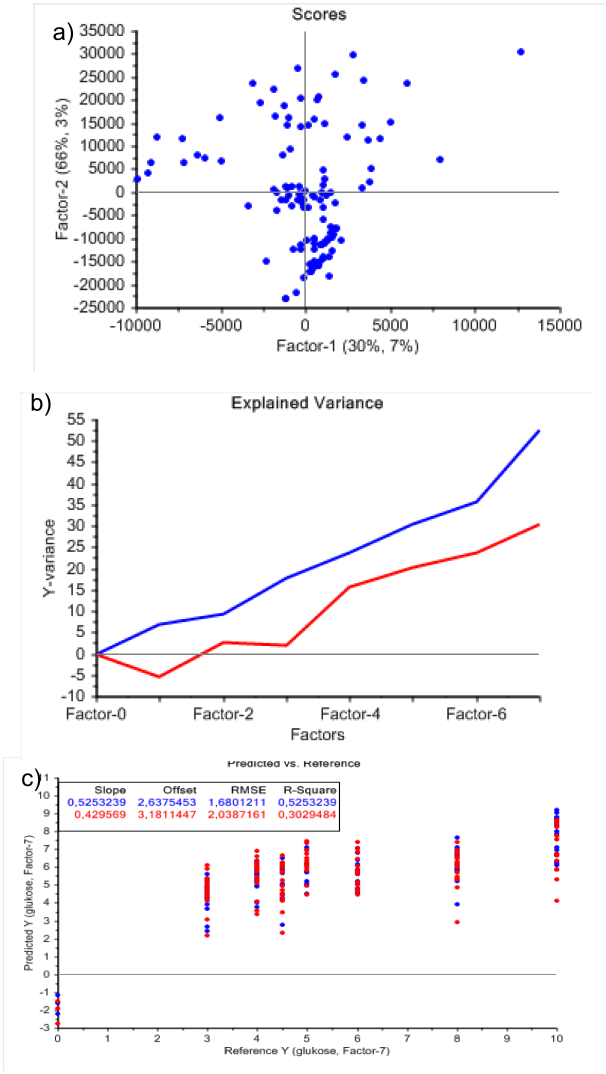

Figure 5.17: PLSR on Raman data did not yield good prediction

5.9 FTIR

Water is removed from the spectra in the sample preparation, however different sample thickness will lead to baseline variations according to Beer-Lamberts law.

Again we use the same general procedure for preprocessing. We perform smoothing by moving average, gap size 11, and perform EMSC correction on the whole spectrum. We performed PLSR on the whole spectrum on patients 1,2 and 3, the PLSR results are seen in figure 5.18.

The first factor is seen to explain 85% of the Y-variance. The predicted values are plotted in section 6. We have also included the predicted values from PLSR, with only difference that it was performed on patients 1,2,3 and 4.

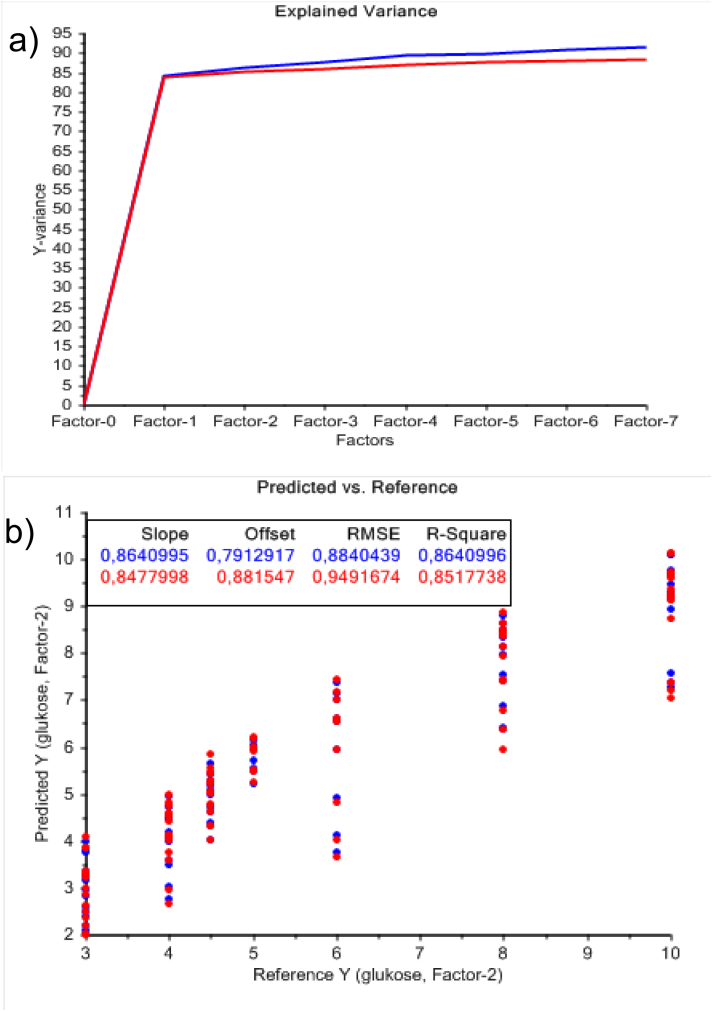

Figure 5.18: a) scores from PLSR, the. b)

6 Results

6.1 Foss 6500

6.1.1 Prediction Using Range From MWPLSR

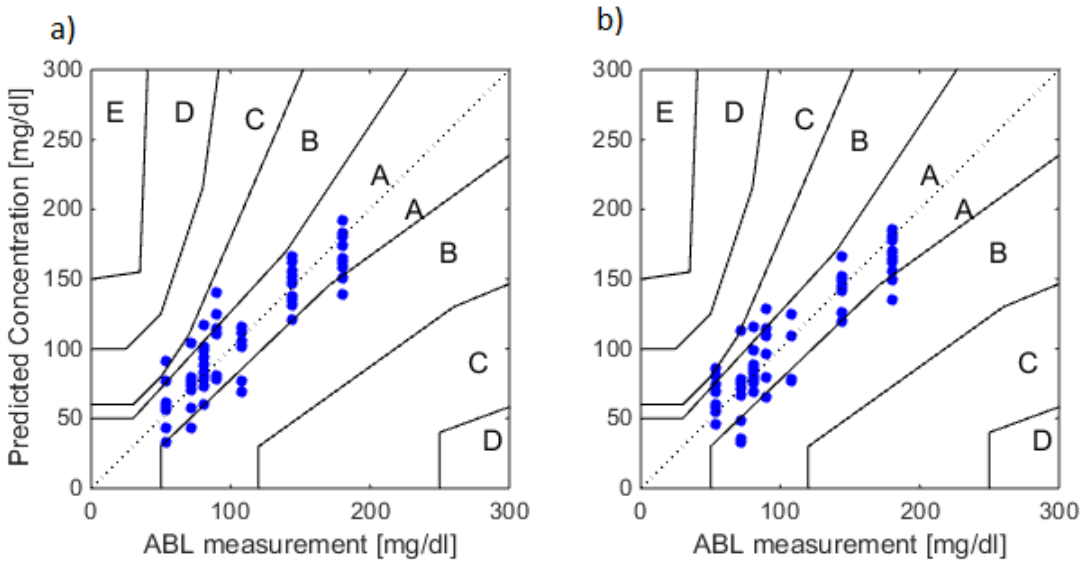

Figure 6.1: Error grid analysis plot of model h and model k

Model h predicted using MW1, both measurement series and preprocessing 2.
Model k predicted using MW1, measurement series 2 and preprocessing 2.

6.1.2 Prediction Using Particular Wavelengths

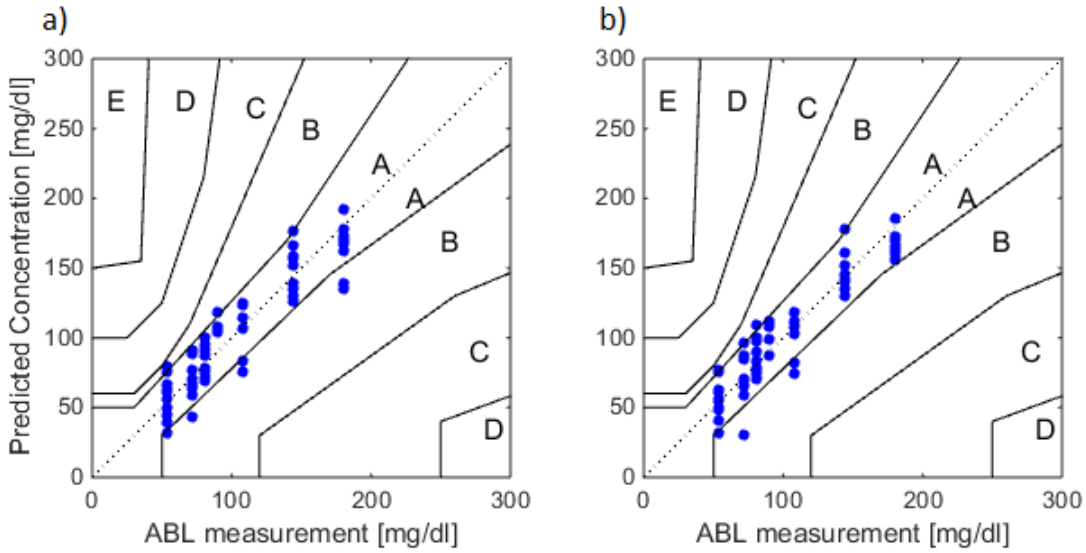

Figure 6.2: Error grid analysis plot of model i and model l

Model i predicted using P1, both measurement series and preprocessing 2.

Model l predicted using P1, measurement series 2 and preprocessing 2.

6.1.3 Training and Test Set

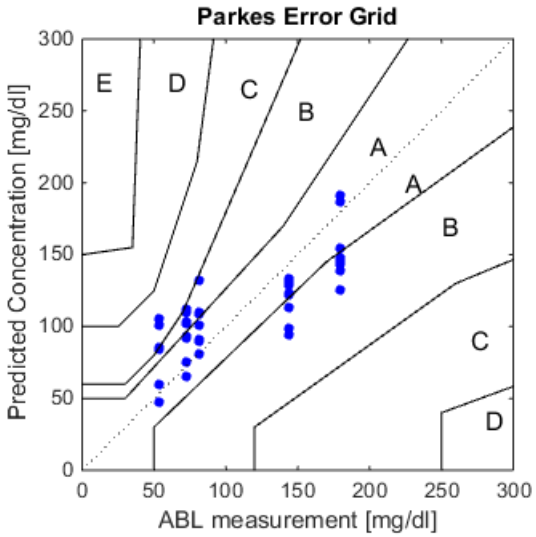

Figure 6.3: Error grid analysis plot of predicted values using patient 2 and 3 as training data, and patient 1 as test data

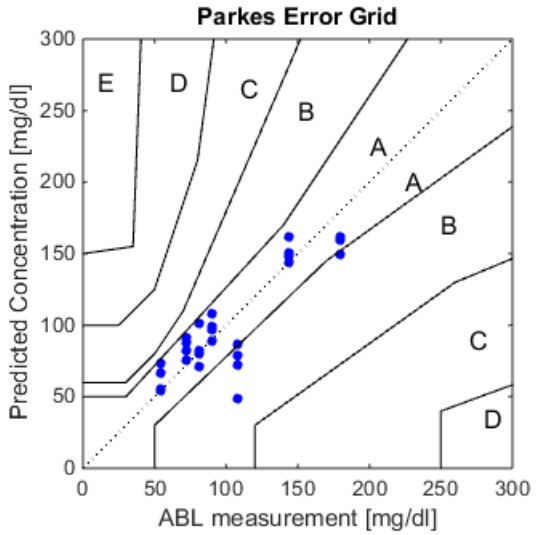

Figure 6.4: Error grid analysis plot of predicted values using patient 1 and 3 as training data, and patient 2 as test data

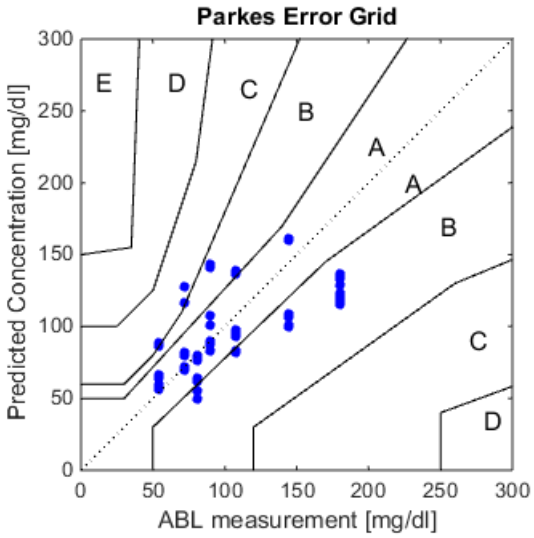

Figure 6.5: Error grid analysis plot of predicted values using patient 1 and 2 as training data, and patient 3 as test data

6.2 XDS

6.2.1 Prediction Using Range From MWPLSR

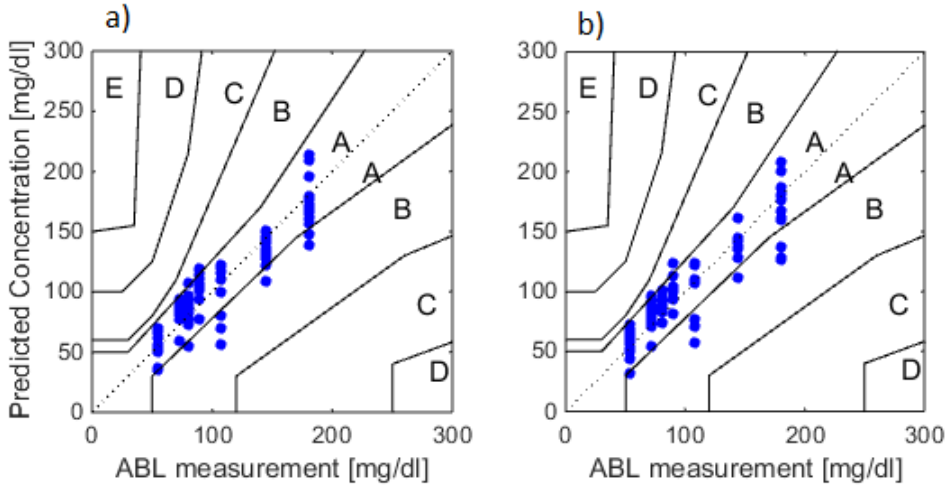

Figure 6.6: Error grid analysis plot of predicted values from model generated from a) preprocessed data b) preprocessed and cuvette adjusted by using MWPLSR wavelengths

6.2.2 Prediction Using Particular Wavelengths

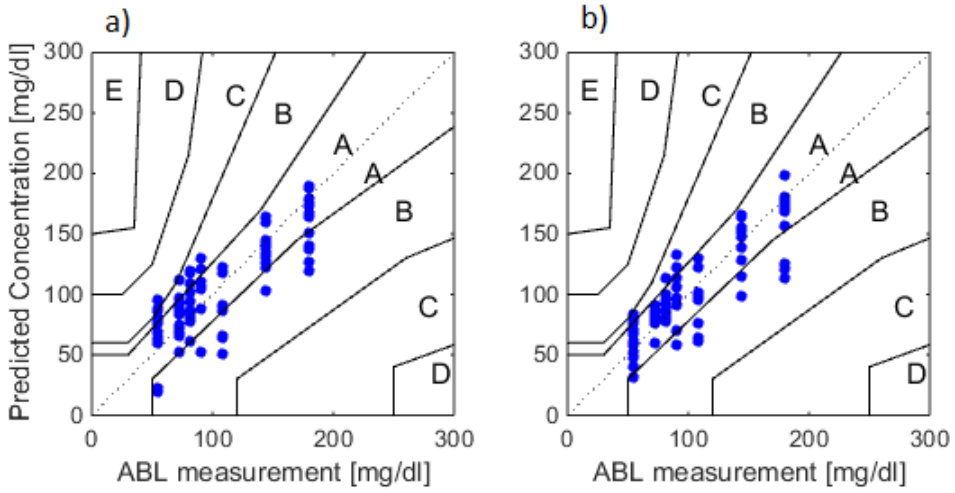

Figure 6.7: Error grid analysis plot of predicted values from model generated from a) preprocessed data b) preprocessed and cuvette adjusted by using MWPLSR wavelengths

6.2.3 Prediction by calibration on single patient

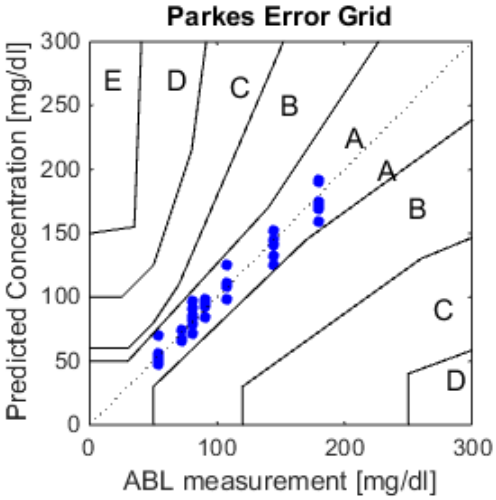

Figure 6.8: Error grid analysis plot of predicted values from model generated from unpreprocessed data using MWPLSR wavelengths.

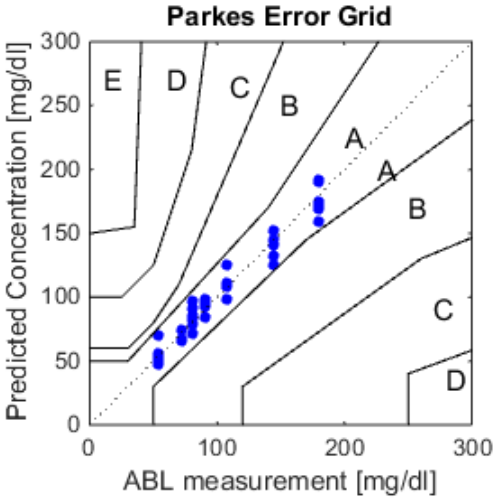

Figure 6.9: Error grid analysis plot of predicted values from model generated from preprcessed and cuvette adjusted data using MWPLSR wavelengths. Bad data removed

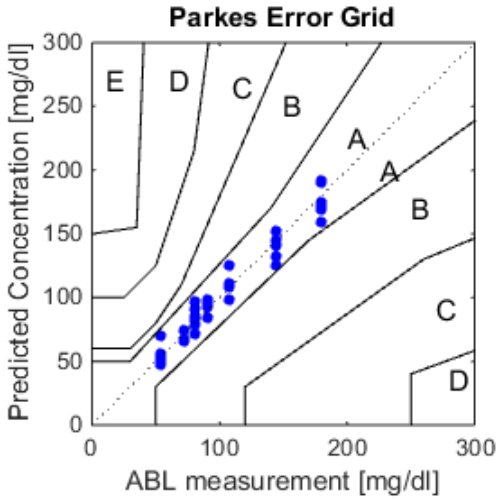

Figure 6.10: Error grid analysis plot of predicted values from model generated from preprcessed and cuvette adjusted data using MWPLSR wavelengths. More bad data removed

6.3 Raman

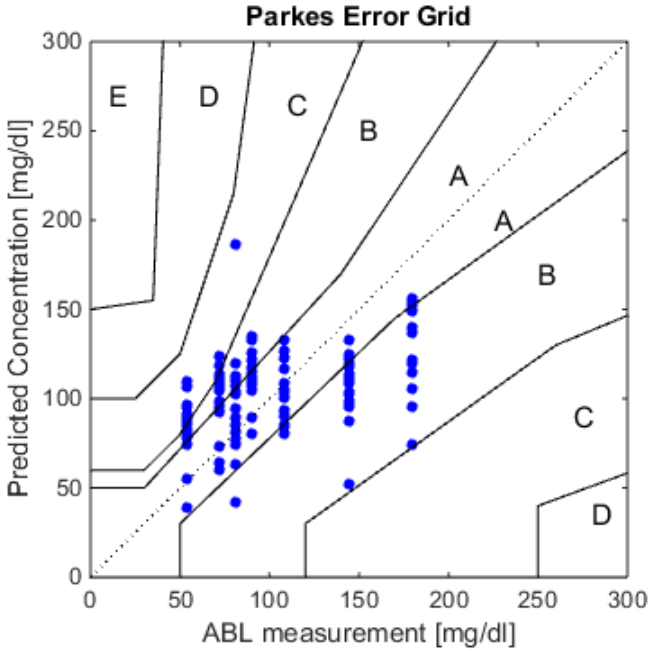

Figure 6.11: Not convincing prediction from Raman data.

6.4 FTIR

6.4.1 Prediction with all patients

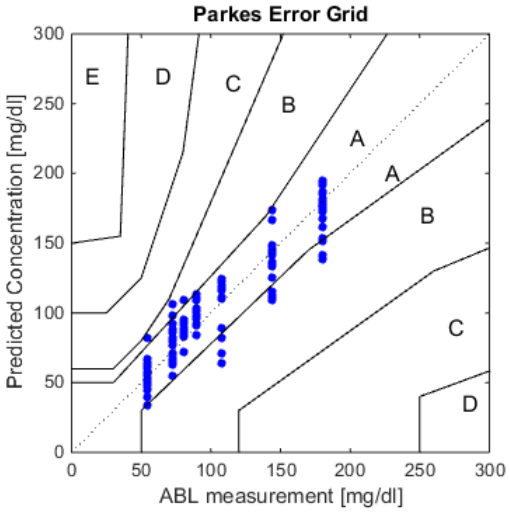

Figure 6.12: The predicted values from PLSR on patient 1,2,3,4

6.4.2 Prediction without patient 4

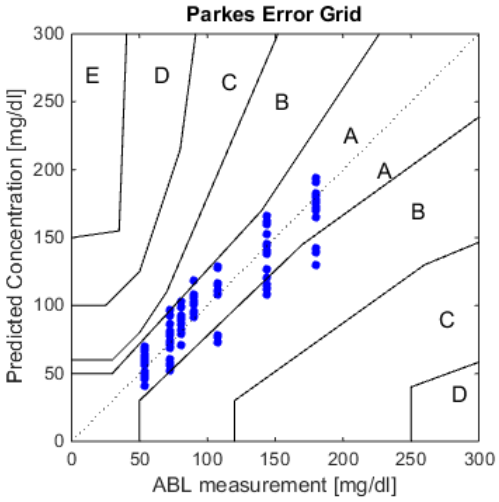

Figure 6.13: The predicted values from PLSR on patients 1,2,3

7 Discussion

The XDS is a newer instrument than FOSS. Apart from that, different measurement setup is used with the two instruments. We used a regular transmission set up at 1 mm pathlength with the XDS, while a dip probe for transflectance measurements at 0.4 mm pathlength was used with the FOSS. The older FOSS showed greater noise characteristic than the XDS, part of this is introduced by the fibre optics, while part of this is due to degradation of instrument parts as it has been in operation since 1994, at least. The better signal-noise ratio in the XDS can to a large degree explain the better results from the PLS regression. The weak signal from glucose absorption is utterly dependent on an excellent signal to noise ratio to obtain any degree of precision at the physiological concentrations.

7.1 IR information

The FTIR and Raman spectras give complementary information. Because the vibrational phenomena that are Raman active are not observed by the FTIR measurments and vice versa. Not studied what informatin is available in the IR region to the same extent as in the NIR region. However, the analysis and results come from the same general procedure that we have applied to the NIR data.

7.2 One or all patients?

The regression models built from the data of one patient give better results than the model generated from all patients. The reason for this could be the variation in the peritoneal composition from patient to patient. This variation may not be adequately compensated for in the generated regression model. More information and data from peritoneal fluid and the variation between

patients are needed to improve the prediction performance. Calibration of the sensor for individual patients should be included in a prediction procedure.

A point in doing EMSC on measurements from single patients. Patient info is considered known and EMSC could represent eventual efforts at incorporating known interferences in the modeling.

The suggested explanation for this is that the observed differences from patient to patient would be in the amount of proteins, and other confounding material, that is analytes which have a spectral signature similar to glucose. Thus PLSR models which are calibrated for this changes should give better overall results.

This would be outside the scope of this thesis, as we have focused on finding specific glucose information. The experiments done here are inadequate as a basis to comment on the presence of these other biological interferents. New experiments are needed to give information on how these interfere with the glucose calibration. This could be done by varying glucose and the other relevant analytes in a factorial design.

7.3 EGA and clinical relevance

The clinical relevance is tested with the EGA plots. Even though the score well in the plots, often the R^2 is not that good. And the RMSECV could be high but still get the results in A and B. The range measured in this study is also to short to get the whole picture of performance in a clinical setting, so future experiments should include a grater range of glucose levels to determine. About 3-20 mmol/l at least.

8 Conclusion

In this study we have investigated the possibility of detecting and quantifying glucose concentration, in the physiological range, in peritoneal fluid samples.

We have developed a protocol to use the FOSS 6500 spectrophotometer for experiments on glucose concentration on peritoneal fluid.

By applying multivariate calibration techniques, we have analysed the acquired data.

From experiments on high glucose concentration and temperature effect, we have found the same interesting spectral regions as suggested in the literature.

Using the MWPLSR procedure we have successfully improved prediction when using the given wavelengths. This results contributes to future research on developing a NIR sensor using specific wavelengths.

While the results from FOSS 6500 are promising, there are certain issues in the predictive ability of the NIR measurements, which we have discussed. We observe similarities when analysing measurements taken with the XDS Metrohm spectrometer.

While the FTIR measurements give good predictions the Raman measurements does not yield any good results.

9 Suggestions for future work

In this work we have hopefully taken a small step towards the goal of a working implantable glucose sensor for the peritoneal cavity, and shed some light on natural next steps towards APT's goal of an artificial pancreas. Some ideas and issues to consider are given here.

Peritoneal fluid samples A priority for future study should be to acquire samples of peritoneal fluid from healthy individuals as well as individuals with diabetes type 1 or type 2. This is necessary in order to confirm or discard the results from the presented experiments. It is not known to what extent the fluid samples used here are representative to peritoneal fluid extracted healthy patients. New experiments should include variations in other interferences as well, e.g. proteins, hemoglobin, fat. A broader range of glucose concentrations, as well as additional values should be considered for future experiments.

Another issue is the storage of the samples from time of extraction until they are measured. Ideally measurements should be done immediately after extraction because biological material will degrade over time. Both measurements by spectroscope and reference method (ABL 725 or other) should be conducted as soon as possible following extraction. A possibility is to freeze the samples to stop the biological processes, however, it is possible that this will have an effect on the glucose measurements.

Peritoneal fluid composition Investigation into what components in peritoneal fluid one could expect to see interferences from in the NIR region. Make an overwiev over what absorption bands glucose share with the other components in peritoneal fluid, and combine this with experimental results from wavelength selection analysis.

Compare measurements in whole blood, blood plasma and peritoneal

fluid to demonstrate the benefits of peritoneum as a measuring site. Ideally in an in-vivo experiment with simultaneous measurments at different locations by NIR sensor, combined with reference measurements with glucoset and blood gas analyser.

Measuring specific wavelengths The measurements taken on Foss 6500 and the XDS instruments, were performed using the instruments auto-gain functionality. This adjusts the gain to match the absorbance of the measured spectra in order to obtain the most spectral information. The water absorption dominates the spectra, and the gain are adjusted accordingly. The pathlength was attempted to be held at a minimum for the transflectance probe, so as to avoid saturation in the spectra. A possibility is to only measure the spectra between the water peaks in the NIR region. Then one could measure at a longer pathlength, thus acquiring more of the weaker absorbance phenomena. This strategy is shown to yield more information for measurements of chloroform, $CHCl_3$, [11]. This could be done with filters or LED sensors.

Miniaturization Miniaturization of a NIR system able to operate inside the peritoneal cavity. Such a system may measure at the suggested wavelength regions, or it may use the discrete wavelengths suggested in a LED array with suitable detectors. LEDs are available in th

Sensor fusion Investigating the possibilities of making a sensor system utilizing multiple sensor technologies. A combination of Raman and NIR and polarimetric sensors should be considered as they are promising candidates for miniaturized systems. Other possibilities for measurements in peritoneal fluid should also be investigated. The benefits from multiple sensor inputs, based on different measuring principles could be exploited in Kalman filtering. Complimentary data from optical methods may con-

tribute to reduce the effect of the nonspecificity of the absorbance methods.

Preprocessing There are a number of different preprocessing techniques that should be investigated for further analysis of the measurements. GLS preprocessing can be used to remove and down-weigh disturbances that are known, prior to measurment, to interfere with the analyte signal. We discussed here the PLSR's ability to model the temperature effect. Temperature will probably not be a great disturbance in the peritoneum. However, other effects may be removed with the benefit of greater prediction accuracy.

Models describing the physiological environment of the sensors should be combined with the application of data driven multivariate calibration models as described in this thesis. This should improve the prediction capabilities of a future implantable sensor.

Knowledge from physical chemistry on the overtone and combination absorbance bands of glucose and confounders should be incorporated into the selsction of optimal wavelengths. This could, in theory, better the specificity of the regression models. And to some extent validate the specificity of the wavelength selection.

10 References

[1] "Key findings 2014 - idf." http://www.idf.org/diabetesatlas/update-2014. [Accessed: 18-12-2014].

[2] A. Trabelsi, M. Boukadoum, and M. Siaj, "A preliminary investigation into the design of an implantable optical blood glucose sensor," *American journal of biomedical engineering*, vol. 1, no. 2, pp. 62–67, 2011.

[3] D. R. Burnett, L. M. Huyett, H. C. Zisser, F. J. Doyle, and B. D. Mensh, "Glucose sensing in the peritoneal space offers faster kinetics than sensing in the subcutaneous space," *Diabetes*, vol. 63, no. 7, pp. 2498–2505, 2014.

[4] F. Chee and T. Fernando, *Closed-Loop Control of Blood Glucose*. LNCIS, Berlin Heidelberg: Springer-Verlag, 2007.

[5] G. Bazar, Z. Kovacs, M. Tanaka, A. Furukawa, A. Nagai, M. Osawa, Y. Itakura, H. Sugiyama, and R. Tsenkova, "Water revealed as molecular mirror when measuring low concentrations of sugar with near infrared light." Manuscript draft submitted to PLOS ONE, 2014.

[6] R. J. McNichols and G. L. Coté, "Optical glucose sensing in biological fluids: an overview," *Journal of Biomedical Optics*, vol. 5, no. 1, pp. 5–16, 2000.

[7] H. E. Frøyen, "Algorithms for closed-loop glucose control in diabetes and intensive-care patients," Master's thesis, Norwegian University of Science and Technology, Trondheim, Norway, 2014.

[8] R. J. Schrot, K. T. Patel, and P. Foulis, "Evaluation of inaccuracies in the measurement of glycemia in the laboratory, by glucose meters, and through measurement of hemoglobin a1c," *Clinical Diabetes*, vol. 25, no. 2, pp. 43–49, 2007.

[9] S. Vaddiraju, D. J. Burgess, I. Tomazos, F. C. Jain, and F. Papadimitrakopoulos, "Technologies for continuous glucose monitoring: Current problems and future promises," *Journal of Diabetes Science and Technology*, vol. 4, no. 6, pp. 1540–1562, 2010.

[10] H. W. Siesler, *Basic Principles of Near-Infrared Spectroscopy*, ch. 2, pp. 7 – 19. CRC Press, 2008.

[11] C. Pasquini, "Near infrared spectroscopy: Fundamentals, practical aspects and analytical applications," *J. Braz. Chem. Soc.*, vol. 14, no. 2, pp. 198–219, 2003.

[12] "Molecular vibration." `http://en.wikipedia.org/wiki/Molecular_vibration`. [Accessed: 19-09-2014].

[13] "Wikimedia commons: Em-spectrum." `http://commons.wikimedia.org/wiki/File:EM_spectrum.svg`. [Accessed: 23-10-2014].

[14] S. Liakat, K. A. Bors, L. Xu, C. M. Woods, J. Doyle, and C. F. Gmachl, "Non-invasive in vivo glucose sensing on human subjects using mid-infrared light," *Biomed. Opt. Express*, vol. 5, no. 7, pp. 2397–2404, 2014.

[15] J. J. Workman and D. A. Burns, *Commercial NIR Instrumentation*, ch. 4, pp. 67 – 78. CRC Press, third edition ed., 2008.

[16] S. Fard, W. Hofmann, P. Fard, G. Böhm, M. Ortsiefer, E. Kwok, M.-C. Amann, and L. Chrostowski, "Optical absorption glucose measurements using 2.3 micron vertical cavity semiconductor lasers," *IEEE photonics tech letters*, vol. 1, no. 11, 2006.

[17] Y. Z. Yu, K. D. Crothal, L. Jahn, and M. DeStefano, "Laser diode applications in a continuous blood glucose sensor," *Proceedings of SPIE*, vol. 4996, pp. 268–274, 2003.

[18] N. Campbell and J. Reece, *Biology*. San Francisco: Pearson education inc. - Benjamin Cummings, 2005.

[19] H. Martens, "Reliable and relevant modelling of real world data: a personal account of the development of pls regression," *Chemometrics and Intelligent Laboratory Systems*, vol. 58, no. 2, pp. 85 – 95, 2001.

[20] H. Martens and T. Næs, *Multivariate Calibration*. Chichester UK: John Wiley & Sons, 1989.

[21] S. Wold, M. Sjöström, and L. Eriksson, "Pls-regression: a basic tool of chemometrics," *Chemometrics and Intelligent Laboratory Systems*, vol. 58, no. 2, pp. 109 – 130, 2001.

[22] "Abl700 series reference manual," tech. rep., Radiometer Medical ApS, 2008.

[23] H. Martens, M. Høy, B. M. Wise, R. Bro, and P. B. Brockhoff, "Pre-whitening of data by covariance-weighted pre-processing," *Journal of Chemometrics*, vol. 17, pp. 1–14, 2003.

[24] H. Martens, J. P. Nielsen, and S. B. Engelsen, "Light scattering and light absorbance separated by extended multiplicative signal correction," *Analytical Chemistry*, vol. 75, no. 3, pp. 394–404, 2003.

[25] J. H. Jiang, R. J. Berry, H. W. Siesler, and Y. Ozaki, "Wavelength interval selection in multicomponent spectral analysis by moving window partial least-squares regression with applications to mid-infrared and near-infrared spectroscopic data," *Analytical Chemistry*, vol. 74, no. 14, pp. 3555–3565, 2002.

[26] C. H. Spiegelman, M. J. McShane, M. J. Goetz, M. Motamedi, Q. L. Yue, and G. L. Coté, "Theoretical justification of wavelength selection in pls calibration: Development of a new algorithm," *Analytical Chemistry*, vol. 70, no. 1, pp. 35–44, 1998.

[27] H. Martens and M. Martens, "Modified jack-knife estimation of parameter uncertainty in bilinear modelling by partial least squares regression (plsr)," *Food Quality and Preference*, vol. 11, no. 1–2, pp. 5 – 16, 2000.

[28] J. L. Parkes, S. L. Slatin, S. Pardo, and B. H. Ginsberg, "A new consensus error grid to evaluate the clinical significance of inaccuracies in the measurement of blood glucose," *Diabetes Care*, vol. 23, no. 8, pp. 1143–1148, 2000.

[29] P. A, K. DC, P. S, and P. JL, "Technical aspects of the parkes error grid," *Journal of Diabetes Science and Technology*, vol. 7, no. 5, pp. 1275–1281, 2013.

[30] M. Golic, K. Walsh, and P. Lawson, "Short-wavelength near-infrared spectra of sucrose, glucose, and fructose with respect to sugar concentration and temperature," *Applied Spectroscopy*, vol. 57, no. 2, pp. 139 – 145, 2003.

[31] K. J. Jeon, I. D. Hwang, S. Hahn, and G. Yoon, "Comparison between transmittance and reflectance measurements in glucose determination using near infrared spectroscopy," *Journal of Biomedical Optics*, vol. 11, no. 1, p. 014022, 2006.

Insert appendix

Appendix A Matlab files

Appendix A.1 MWPLSR.m

```
function SSR=MWPLSR(D,P)
% input: D: data matrix of measured samples
%        P: plot flag
% out:   SSR: matrix of the sum of square of residuals
   from the PLSR model
% calculated at each
% wavelength at the given window size for 1 to 7 factors.
%
if nargin < 2
    P=0;
end

%indexes of patient samples in data matrix
%XDS
p1 = 4:1:33;
p2 = [51:55,59:61,65:67,74:76,92:94,113:114];
p3 = [37,38,39,43,44,45,46,47,62,63,64,68,69,...
    70,71,72,73,77,78,79,80,81,82,83,84,85,95,...
    97,99,100,104,105,106,110,111,112];

%FOSS
Fp1 = [1:2,13:16,19:20,27:28,31:32,43:48,...
    51:52,90:91,100:101,104:107,122:123,...
    144:145,148:149,152:157];
Fp2 = [5:6,17:18,23:26,37:38,41:42,67:68,...
    92:97,120:121,134:135,140:141,146:147];
Fp3 = [3:4,9:12,21:22,29:30,39:40,49:50,...
    53:54,59:62,65:66,69:74,84:89,102:103,...
    110:115,118:119,124:133,138:139,150:151];

start_ind=7;
glucose_ind=5;
S2 = 1020;
nm = 430:2:2468;
Y=D(:,glucose_ind);
SSR = zeros(S2,7);

%MWPLSR loop
```

```
38 h=waitbar(0);
39 for j = 1:S2
40
41     a = start_ind+(j-1);
42     b = a + 30;
43
44     X=D(:,a:b);
45
46     for i = 1:7
47         [~,~,~,~,~,~,MSE,stats] = plsregress(X,Y,i);
48         SSR(j,i)=log(sum(stats.Yresiduals.^2));
49     end
50     waitbar(j/S2)
51 end
52 close(h)
53
54 if P
55     figure
56     plot(nm,SSR,'LineWidth',1);
57     ylabel('log SSR','FontSize',14,'FontWeight','bold');
58     xlabel('Wavelength','FontSize',14,'FontWeight','bold'
       );
59 end
```

Appendix A.2 parkes.m

```
function parkes(y,yp)


% calculate mg/dl
y=y.*18;
yp=yp.*18;


% ------------------------------ Plot Error Grid
    --------------------------------
h = figure;
plot(y,yp,'bo','MarkerSize',4,'MarkerFaceColor','b','
    MarkerEdgeColor','b');
hold on


xlabel('Reference Concentration [mg/dl]');
ylabel ('Predicted Concentration [mg/dl]');
title('Parkes Error Grid');
set(gca,'XLim',[0 550]);
set(gca,'YLim',[0 550]);
axis square

%plot zone limits from: "Technical Aspects of the Parkes
    Error Grid", Pfutzner et al. 2013.
% diagonal
plot([0 550],[0 550],'k:')
% B lower
plot([50 50 170 385 550],[0 30 145 300 450],'k-')
% B upper
plot([0 30 140 280 430],[50 50 170 380 550],'k-')
% C lower
plot([120 120 260 550],[0 30 130 250],'k-')
% C upper
plot([0 30 50 70 260],[60 60 80 110 550],'k-')
% D lower
plot([250 250 550],[0 40 150],'k-')
% D upper
plot([0 25 50 80 125],[100 100 125 215 550],'k-')
% E upper
plot([0 35 50],[150 155 550],'k-')
```

```
39
40 text(10,270,'E','FontSize',12);
41 text(60,270,'D','FontSize',12);
42 text(110,265,'C','FontSize',12);
43 text(150,250,'B','FontSize',12);
44 text(200,225,'A','FontSize',12);
45 text(225,200,'A','FontSize',12);
46 text(250,170,'B','FontSize',12);
47 text(270,90,'C','FontSize',12);
48 text(280,35,'D','FontSize',12);
49
50
51 set(h, 'color', 'white');
52 % sets the color to white
53
54 set(gca,'XLim',[0 300]);
55 set(gca,'YLim',[0 300]);
```